The Influence of Cloud Feedbacks on Equatorial Atlantic Variability

Katinka Bellomo[1], Amy C. Clement[1], Thorsten Mauritsen[2], Gaby Rädel[2], Bjorn Stevens[2]

1. Rosenstiel School of Marine and Atmospheric Science, University of Miami, Miami, FL, USA

2. Max Planck Institute for Meteorology, Hamburg, Germany

[1] *Corresponding author address:* Katinka Bellomo, Rosenstiel School of Marine and Atmospheric Science, University of Miami, 4600 Rickenbacker Causeway, Miami, FL 33149.
Email: kbellomo@rsmas.miami.edu

Abstract

Prior studies have provided observational evidence that cloud feedback over the Namibian stratocumulus region is positive because cloud cover is anti-correlated with local Sea Surface Temperature (SST) anomalies. Moreover, regressions of observed atmospheric fields on equatorial Atlantic SST anomalies indicate that cloud feedbacks over the Namibian stratocumulus region co-vary with Atlantic Niño. However, from observations alone it is not possible to quantify the influence of regional cloud feedbacks on equatorial climate variability. To address this question, a set of sensitivity experiments are conducted using an atmospheric general circulation model (ECHAM6) coupled to a slab-ocean in which the strength of positive cloud feedback is enhanced over several regions in the South Atlantic basin. Enhanced positive cloud feedback over the Namibian stratocumulus region increases local as well as equatorial SST variability, whereas enhanced cloud feedback over other regions in the South Atlantic increases local SST variability but exhibits negligible responses at the equator. Our results indicate that the Namibian region plays a central role in enhancing equatorial SST variability because it is located where the SST anomalies associated with the simulated Atlantic Niño in the slab-ocean model develop. These results highlight the important role of the regional coupling of cloud cover over the Namibian region with local SSTs, and its effects on large-scale atmospheric circulation and equatorial Atlantic climate variability.

1. Introduction

Equatorial Atlantic Sea Surface Temperature (SST) variability is dominated by the annual cycle. SSTs reach their maximum during boreal spring (March-April) when the equatorial trades weaken and the thermocline deepens. As the year progresses, SSTs cool due to the seasonal intensification of the trades and consequent shoaling of the thermocline, reaching their minimum during boreal summer (July-August) (for a review, see Xie and Carton 2004). The Inter-Tropical Convergence Zone (ITCZ) over the ocean follows the annual cycle of SST: it sits over the equator between 10ºS-5ºN during March-April when SSTs are warmest, then it moves north of the equator when the cold tongue develops in June and persists through September (Mitchell and Wallace 1992; Biasutti et al. 2003; Grodsky and Carton 2003).

Departures from the annual cycle of SST occur primarily during boreal summer (June-July-August) over the cold tongue region (6ºS-2ºN, 20ºW-5ºE). These anomalies are accompanied by changes in atmospheric and oceanic circulations that resemble those associated with El Niño Southern Oscillation (ENSO) in the Pacific Ocean, and have therefore been referred to as "Atlantic Niño" events (Merle 1980; Hisard 1980). Atlantic Niños are characterized by warm anomalies along the equator and the eastern side of the South Atlantic Ocean (Ruiz-Barradas et al. 2000), weakening of equatorial trade winds west of 20ºW, and weakening of meridional winds associated with the North African summer monsoon to the east of 20ºW (Horel et al. 1986; Zebiak 1993; Xie and Carton 2004). During warm Atlantic Niños, equatorial deep convection shifts southward (Wagner and da Silva 1994; Carton et al. 1996) and precipitation increases over the Gulf of Guinea (Hirst and Hastenrath 1983). Like their Pacific counterparts, Atlantic Niños have impacts on sea level, precipitation over surrounding continents, and fisheries (Brundrit 1995; Hagen et al. 2001, Boyer et al. 2001). For these reasons,

understanding the origin, dynamics, and the physical mechanisms of SST variability over the equatorial Atlantic is of primary importance to improve the predictability of Atlantic Niños and their impacts.

Using Empirical Orthogonal Function (EOF) analysis, Joint EOF, and Singular Value Decomposition (SVD) methods, previous studies have shown that the dominant modes of variability in the tropical Atlantic Ocean are a zonal mode (i.e., Atlantic Niño) and an inter-hemispheric Atlantic Meridional Mode (among others: Servain 1991; Servain et al. 1999; Nobre and Shukla 1996; Chang et al. 1997; Penland and Matrosova 1998; Tanimoto and Xie 2002; Chiang and Vimont 2004). However, it is still unclear whether the North Atlantic is correlated with Atlantic Niños and South Atlantic variability through the inter-hemispheric mode and on which timescales that mechanism operates (Mehta 1998; Enfield and Mestas-Nunez 1999; Dommenget and Latif 2000).

A number of studies contend that the Atlantic Meridional Mode is an artifact of the statistical methods used to analyze SST correlations. A rotation of the first few EOFs, which relaxes the orthogonality constraint of the normal EOF analysis, shows two leading EOFs each confined to one hemisphere with little projection on the other hemisphere (Houghton and Tourre 1992; Dommenget and Latif 2000; Trzaska et al. 2007). The Atlantic cold tongue is more influenced by the South Atlantic because of the geometry of the African continent and because the climatological position of the ITCZ in the northern hemisphere predominantly drives surface cross-equatorial flow from the south to the north, which means that perturbations in the trade winds in the northern hemisphere have relatively little influence on equatorial SSTs as it has been shown for the Pacific (cf. Okumura 2013; Zhang et al. 2014b; Bellomo et al. 2014b). For these reasons, it is argued that Atlantic equatorial variability is more strongly influenced by

93 South Atlantic rather than North Atlantic SST variability (Dommenget and Latif 2000; Trzaska
94 et al. 2007).

95 Several studies have shown connections between the subtropical and extra-tropical South
96 Atlantic and equatorial Atlantic variability (Venegas et al. 1996; Robertson et al. 2003, Barreiro
97 et al. 2004). These can be divided into studies that argue for a fundamental role for oceanic
98 processes and ocean waves (among others, Zebiak 1993; Carton et al. 1996; Delecluse et al.
99 1994; Servain et al. 1999; Sutton et al. 2000; Florenchie et al. 2003; Florenchie et al. 2004), and
100 studies that contend that thermodynamic feedbacks involving the interaction of atmospheric
101 circulation, latent heat flux, and cloud cover can alone explain tropical Atlantic variability and to
102 the first order, Atlantic Niño (among others, Dommenget and Latif 2000; Tanimoto and Xie
103 2002; Haarsma et al. 2003; Sterl and Hazeleger 2003; Chaves and Nobre 2004; Trzaska et al.
104 2007, Evan et al. 2013).

105 Dommenget and Latif (2000) used a hierarchy of climate models to show that a positive
106 feedback among SST, wind stress, and latent heat flux at the surface is more important than
107 ocean dynamics in driving upper ocean tropical Atlantic variability. In addition, a number of
108 studies, including Tanimoto and Xie (2002), Park et al. (20005), Trzaska et al. (2007), and Evan
109 et al. (2013), have shown the importance of positive cloud feedbacks in increasing the
110 persistence of SST anomalies over low-level cloud regions located off the coasts of Namibia. For
111 example, Evan et al. (2013) estimated the influence of low-level cloud feedback from
112 observations, and then showed with an idealized coupled linear model that cloud feedbacks are
113 necessary for the SST anomalies associated with simulated Atlantic Meridional Mode to persist
114 as long as in observations.

Using observations, idealized climate models, and theoretical frameworks, these previous studies showed evidence that local coupling between SSTs and cloudiness can influence large-scale climate variability in the South Atlantic Ocean. However, those studies did not evaluate the impacts of cloud feedbacks relative to other atmospheric or oceanic processes, or the influence of cloud feedbacks from different regions over the South Atlantic basin.

To address these questions, we use an atmospheric general circulation model (ECHAM6) coupled to a slab-ocean in which we artificially increase the strength of positive cloud feedback over selected regions. First, we investigate the role of cloud feedbacks over the Namibian stratocumulus region in modulating the persistence of local and equatorial SST variability, and then we evaluate the influence of cloud feedbacks from other regions in the South Atlantic on equatorial SST variability.

2. Data and methods

a. Observations

We use monthly mean values of Sea Surface Temperature (SST) from the Extended Reconstructed SST reanalysis (ERSSTv3b; Smith et al. 2008) along with surface winds and Sea Level Pressure (SLP) from the NCEP/NCAR reanalysis (Kalnay et al. 1996). Observed cloud feedback is estimated using cloud cover and Cloud Radiative Effect (CRE). We use monthly mean values of cloud cover from the International Satellite Cloud Climatology Project (ISCCP; Rossow and Schiffer 1999) for the years 1984-2007, and seasonal mean values of cloud cover from the Extended Edited Cloud Reports Archive (EECRA; Hahn and Warren 1999, 2009) for the years 1954-2008. Monthly mean values of CRE are from the Clouds and Earth's Radiant

Energy System (CERES) Energy Balanced and Filled (EBAF_Ed2.7) data set for the years 2001-2010 (Loeb et al. 2009), and from ISCCP for the years 1984-2007.

We de-trend all observational data by removing the least squares regression line, and compute monthly mean anomalies by subtracting the long-term monthly mean from each calendar month. For cloud data from EECRA we compute seasonal mean anomalies subtracting the long-term seasonal mean from each season. Observational datasets are affected by observational errors. In satellite data, errors are mostly caused by replacement of instruments and orbital drifts over time. Instead, in ship-based data errors arise due to unknown observational artifacts that introduce a spurious trend in the tropical mean long-term variability (Norris 2005; Eastman et al. 2011; Clement et al. 2009). For these reasons, all cloud datasets were corrected for spurious artifacts by removing tropical mean variability (cf. Bellomo et al. 2014a).

b. Model experiments

To test the role of positive cloud feedbacks on Atlantic climate variability, we perform a series of model experiments using a state-of-the-art AGCM (ECHAM6, v. 6.1.04) coupled to slab-ocean for the open ocean and a thermodynamical sea ice model (Stevens et al. 2013). We use the coarse-resolution (ECHAM6-CR) with T31 horizontal grid (3.75^{o} x 3.75^{o}) and 31 vertical levels. The mixed-layer depth of the slab-ocean model is fixed to 50 m everywhere and does not vary seasonally. In the slab-ocean configuration, interactive ocean dynamics are absent and internal climate variability is driven solely by the thermal coupling between the ocean and the atmosphere (i.e., short- and long-wave radiation plus latent and sensible heat fluxes). The monthly climatology of ocean heat transport (commonly referred to as "q-flux") is prescribed to maintain the SST climatological mean, but does not vary from year to year. For all experiments,

the q-flux is obtained from a control simulation using the AGCM with fixed climatological monthly mean SSTs computed from observations.

We perform a control simulation using the prescription of Coupled Model Intercomparison Project phase 5 (CMIP5) pre-industrial control experiments (Taylor et al. 2012), which we compare with model experiments in which we increase the strength of local positive cloud feedbacks. To increase the strength of positive cloud feedback, we use the experimental design of Bellomo et al. (2014b). Following their method, we multiply cloud liquid water in the radiation module by an amplifying factor "y", which is a function of underlying SST anomalies:

$$y = 1 - \arctan(\mathrm{SST}) * 2/\pi \quad (1)$$

In the equation above, SST indicates local SST anomalies computed as SST in the current run minus SST monthly mean climatology computed from a control simulation. Eq. (1) is applied at each time step of the model simulation and at each grid point where we increase the strength of local positive cloud feedback. In this study positive feedback means a reduction (increase) in cloud radiative effect when the underlying SST anomaly is warm (cold). Refer to Bellomo et al. (2014b) for further details of the model setup.

We perform a first experiment in which cloud feedback is enhanced in the subtropical South Atlantic where the mean subsidence at 500 hPa is greater than 10 hPa day^{-1} and the mean Lower Tropospheric Stability (LTS) is greater than 16.5 K (LTS is defined as the difference in potential temperature at 700 hPa and the surface). These criteria are chosen to target regions in which subtropical stratocumulus clouds predominate in the model (Medeiros and Stevens 2011). The box in which these constraints are met in the model is highlighted in red in fig. 1 and corresponds to the Namibian stratocumulus region (Klein and Hartmann, 1993). Hereafter, we

will refer to the experiment that enhances cloud feedbacks in this region as the "Namib" simulation. Both the Control and the Namib simulations are run for 200 years.

To investigate the role of cloud feedbacks over other South Atlantic regions, we perform a series of sensitivity experiments in which we enhance the strength of positive cloud feedback in nine regions located within 5ºN-30ºS, 40ºW-10ºE. These experiments are named according to the number in the black boxes in fig. 1 (e.g., "Box 1", "Box 2", etc.), where we note that Box 6 is a subset of the Namib experiment. We run all sensitivity experiments for a period of 100 years. The length of these simulations is motivated both by computational resources and the fact that the analysis of 80 years instead of 180 years in the control and Namib experiments leads to qualitatively similar results. The analysis of the nine experiments in the boxes motivated longer simulations for Box 3 and Box 6, which were run for an additional 50 years (i.e., a total of 150 years of simulation time). We use these longer experiments to further characterize the influence of these regions on low-frequency equatorial variability.

For all experiments, we discard the first 20 years of spin-up time from the analysis to remove the possible influence of the initial conditions, and we compute monthly mean anomalies by removing the simulated annual cycle from each month. For all slab-ocean experiments shown in this paper we find that the global mean change in SST from the control simulation is negligible (order of ~0.01). Moreover, Bellomo et al. (2014b) showed that changes in the mean climate do not affect the changes in internal climate variability caused by enhanced cloud feedbacks and the simulation of the seasonal cycle of SST.

3. Results

a. Observations

205 Figure 2 shows the regressions of observed local (shaded) SST anomalies, (contours) SLP, and
206 (vectors) surface winds on the Atl3 index for the years 1960-2010. The Atl3 index (5ºS-5ºN,
207 20ºW-0ºE), which is highlighted by the black box in fig. 2, is an index of SST anomalies that is
208 used to measure Atlantic Niño activity. Stippling in fig. 2 indicates where the linear correlation
209 of SST with the Atl3 index is statistically significant at the 95% level of a Pearson's R test for
210 correlations.

211 The regression in fig. 2 displays a zonal mode along the equator that is commonly
212 referred to as Atlantic Niño. Atlantic Niño is accompanied by large anomalies in the strength of
213 trade winds along the equator and northerly wind anomalies crossing the equator (fig. 2). A
214 weakening of SLP and wind circulation around the subtropical high is evident in the South
215 Atlantic. Atlantic Niño is correlated with SST anomalies of the same sign in the southeastern
216 part of the South Atlantic Ocean, and with SST of opposite sign in the southwest. It is
217 noteworthy that Atlantic Niño SST anomalies are significantly correlated with SSTs in the South
218 Atlantic Ocean (stippling in fig. 2), but not correlated with North Atlantic SSTs, suggesting that
219 Atlantic Niños are influenced by South Atlantic SSTs but not by North Atlantic SSTs and the
220 Atlantic Meridional Mode (see discussion in Marshall et al. 2001).

221 Atlantic Niño is also accompanied by large changes in cloud cover, which influence the
222 radiation budget at the surface. To calculate the anomalies in the net radiation budget at the
223 surface due to changes in cloud cover, we estimate cloud amount feedback as defined in Bellomo
224 et al. (2014a) from observations. To estimate cloud amount feedback, we first divide
225 climatological mean net (i.e., long-wave plus short-wave) Cloud Radiative Effect (CRE) by
226 climatological mean total cloud amount, where CRE is computed as the difference between total-
227 sky and clear-sky radiation fluxes at the surface. This ratio is called "cloud amount radiative

kernel" (k) as in Bellomo et al. (2014a), and represents the sensitivity of CRE to changes in mean cloud amount (units of W m^{-2} $\%^{-1}$):

$$k = \frac{\overline{\bar{C}\bar{R}\bar{E}}}{\bar{C}} \qquad (2)$$

Cloud amount radiative kernel is computed using radiative fluxes from CERES using the years 2001-2009 and all years available for cloud data in the two cloud datasets. Then, we multiply the cloud amount radiative kernel (eq. 2) by the regression of total cloud amount on the Atl3 SST index anomalies to obtain the regression of cloud amount feedback on the Atl3 SST index (units of W m^{-2} K^{-1}). As discussed in Bellomo et al. 2014a, cloud amount feedback as estimated here does not take into account perturbations in cloud vertical and optical properties and should be interpreted as the cloud amount component of the total cloud feedback, which can be written as the sum of cloud amount, cloud altitude, cloud optical feedbacks, and a residual term (Zelinka et al. 2012).

The regressions of cloud amount feedback on Atl3 SST index are shown in fig. 3. Fig. 3a is obtained using cloud data from ISCCP for the years 1984-2007, while fig. 3b is obtained using cloud data from EECRA for the years 1954-2008. These regressions represent the net radiation anomaly at the surface that is due to changes in cloud cover associated with Atlantic Niño SST fluctuations. Changes in cloud cover (contours) display a decrease in the eastern part of the South Atlantic, which is mostly covered by low-level stratocumulus clouds, and an increase in cloud cover in the western equatorial Atlantic, where deep-convective clouds are predominant. The decrease in low-level clouds in the eastern part of the basin associated with warm SST anomalies in the Atl3 region is interpreted as a positive cloud amount feedback (shaded) that further amplifies SST anomalies (cf. Evan et al. 2013). In contrast, the increase in deep-convective clouds in the western equatorial Atlantic is interpreted as a negative cloud amount

feedback, which damps underlying warm SST anomalies (fig. 2). Therefore, a positive cloud feedback associated with low-level clouds in the eastern part of the basin promote the persistence of SST anomalies associated with the Atl3 region (fig. 2), whereas negative cloud feedback due to deep-convective clouds in the western equatorial Atlantic damps SST anomalies.

The negative values of the regression of cloud amount feedback on Atl3 SST index found over the southwestern part of the basin (fig. 3) also represent a positive cloud feedback because SST anomalies are negative in this region when Atl3 anomalies are positive (cf. fig. 2). That is, cooler SSTs over the southwestern South Atlantic are associated with more cloud cover (contours), and hence less radiation into the surface. Observations from ships (fig. 3b) are coarser and sparser but do resemble the large-spatial pattern seen from satellites (fig. 3a). Most importantly, they show that these changes in cloud cover are not particular to the satellite era, suggesting that they are not related to trends or biases in the ISCCP dataset (Bellomo et al., 2014a).

Observations over the last six decades show that clouds co-vary with SST in the Atl3 region and with atmospheric large-scale circulation in a way that would amplify SST anomalies over the Namibian stratocumulus deck anda the eastern equatorial basin– how does this cloud radiative forcing influence the variability of Atlantic Niño?

b. Role of cloud feedbacks over the Namibian region

To investigate the role of cloud feedbacks on Atlantic Niño and large-scale modes of climate variability, we run model experiments in which we enhance positive cloud feedback over the Namibian region, as outlined in Section 2. Differently from observations, cloud feedback is estimated in model simulations as the regression of net CRE at the surface on local SST. This

273 definition is different from the cloud amount feedback estimate shown for observations in fig. 3
274 for two reasons. First, local cloud feedback is used to highlight the response of the model to the
275 imposed cloud liquid water-SST relationship (eq. 1), whereas the observed regressions in fig. 3
276 show cloud radiative effect associated with anomalies in the Atl3 SST index to understand the
277 variability associated with the Atlantic Niño. Second, in the model we compute cloud feedback
278 using radiative fluxes instead of cloud amount. We cannot use cloud amount as we do for
279 observations because we do not change the coupling between cloud amount and SST, but rather
280 between CRE and SST. Nevertheless, changing CRE in response to SST anomalies has the same
281 effects as changing cloud amount. In fact, the regression of CRE on the Atl3 SST index using
282 CRE from the short CERES dataset (2001-2009) and from ISCCP (1984-2007) gives
283 qualitatively similar results to those shown in fig. 3 (not shown).

284 Figure 4a shows the difference in cloud feedback between the Namib experiment, in
285 which we enhance positive cloud feedback over the Namibian stratocumulus region, and the
286 control run. For comparison, fig. 4b shows cloud feedback in the control run, while fig. 4c and
287 4d show observational estimates of cloud feedback using CRE at the surface from CERES
288 (2001-2009) and ISCCP (1984-2007). As intended, the model simulates stronger positive cloud
289 feedback over the stratocumulus deck off the coasts of Namibia (fig. 4a) where we enhance it
290 (black box). There is also a decrease in the strength of cloud feedback in the equatorial regions
291 due to dynamical adjustments in the model. The equatorial response seems to be related to the
292 Wind-Evaporation-SST (WES) feedback (Zhou and Carton 1998). In fact, enhanced cloud
293 feedback over the Namibian region causes a local reduction in the regression of LHF on SST,
294 which in turn causes an increase in the regression of LHF on SST at the equator downwind of the
295 Namibian region presumably due to the WES feedback. The increase in the regression of LHF on

296 SST at the equator is locally balanced by a decrease in cloud feedback. We further investigate
297 these mechanisms by running a set of experiments where we impose a +1K SST anomaly over
298 the Namibian region in a AGCM simulation with fixed SSTs. In those experiments (not shown)
299 we find that mean LHF changes were consistent with a downwind propagation (WES feedback)
300 and were balanced by opposite sign changes in mean CRE (cf. Dommenget et al. 2000).

301 The imposed relationship of cloud liquid water to SST (eq. 1) in the Namib experiment
302 makes the model simulation of cloud feedback more similar to observations. In the control
303 simulation (fig. 4b) cloud feedback is underestimated over the Namibian region and
304 overestimated over the equator, where observations show cloud feedback of negative sign while
305 in the model the sign is positive (cf. with fig. 4c and 4d). In the Namib experiment, cloud
306 feedback over the Namib region shows values of cloud feedback that are stronger and more
307 similar to observations, while over the equator it shows smaller but still positive cloud feedback.
308 We note that we enhance cloud feedback where the model simulates stratocumulus clouds (black
309 box in fig. 4a), which does not necessarily coincides where stratocumulus clouds occur in the
310 real world, as shown by Medeiros and Stevens (2011). We also note that there are uncertainties
311 in observations because CERES exhibits smaller values of cloud feedback estimated as
312 regression of CRE on SST than ISCCP over the eastern part of the basin and larger negative
313 values over the equator.

314 Although there are still differences between the simulations and observations especially
315 along the equator, the simulation of cloud feedback in the Namib experiment is closer to
316 observations and helps us interpret the role of cloud feedbacks in regulating SSTs. Moreover,
317 since we only enhance cloud feedback, these experiments are helpful to separate the role of cloud
318 feedbacks on the simulated internal climate variability from other processes.

319 The effect of increasing the strength of the positive cloud feedback over the Namibian
320 region (fig. 4a) is an overall increase in the variance of SST and SLP (fig. 5), both locally where
321 the feedback is enhanced, and remotely in the equatorial regions. Figures 5a and 5c show the
322 climatological mean SST and SLP variance, respectively. Compared to the climatological mean,
323 the Namib experiment displays enhanced variance of both SST and SLP as shown by the ratio of
324 variance of SST and SLP in the Namib experiment to the control run in fig. 5b and 5d,
325 respectively. In the control simulation the variance of SLP (fig. 5c) resembles observations (not
326 shown) but is smaller than observations over the Namibian region, while the variance of SST
327 (fig. 5a) is smaller than observations (not shown) both over the Namibian region and the
328 equatorial Atlantic due to the absence of ocean dynamics in the slab-ocean configuration
329 (Clement et al. 2011). It is noteworthy that the increase in the strength of cloud feedback over the
330 Namibian region alone can more than double equatorial variability and make the variance of SST
331 and SLP are more similar to observations.
332 Another important effect of enhanced cloud feedback over the Namibian region is an
333 increase in the persistence of SST anomalies as measured by the *e*-folding timescale, which is
334 defined as the month at which the autocorrelation of local SST anomalies drops below a value
335 equal to or smaller than 1/*e* at each grid point. Figure 6 shows the *e*-folding timescale in the
336 control simulation (fig. 6a) and the difference in *e*-folding timescale between the Namib
337 experiment and the control simulation (fig. 6b). In the control simulation the largest *e*-folding
338 time is found off the coasts of Namibia (fig. 6a), while in the Namib experiment the largest
339 increase occurs at about 5ºS of the equator in the eastern part of the basin (fig. 6b). Interestingly,
340 the variance of SST and SLP, and the *e*-folding time, are all enhanced in near-equatorial regions
341 far away from where cloud feedback is increased.

342 The remote influence of cloud feedbacks in the subtropics on equatorial SST indicates
343 that regional cloud feedbacks are connected to large-scale atmospheric circulation and climate
344 variability patterns. In particular, cloud fluctuations and their influence on local SST in the
345 Namibian region are connected to equatorial climate variability. To understand this influence as
346 a function of timescale, we compute power spectra of SST anomalies averaged over the Atl3
347 region in the (black) control simulation and (red) Namib experiment in fig. 7. Black markers on
348 the red curve (Namib experiment) indicate where the difference in variance from the control run
349 is statistically significant at the 95% level of a Fisher's F-test for variances. Figure 7 shows that
350 positive cloud feedback over the Namibian stratocumulus deck significantly increases the
351 variance of equatorial SST anomalies at inter-annual to decadal timescales.
352 We perform an Empirical Orthogonal Function (EOF) analysis on South Atlantic SST
353 variability (40ºS-10ºN, 50ºW-20ºE) in the control and Namib simulations (not shown). The first
354 EOF exhibits a mode of variability as the one seen from observations (fig. 2) and explains 16.4%
355 of the variance. This mode of variability is referred to the South Atlantic Dipole in the literature
356 (e.g., Trzaska et al. 2007) and explains ~20% of SST variance in observations (not shown). The
357 first EOF in the Namib experiment also exhibits the same mode, but explains a larger variance
358 (23.3 %) at the equator due to the enhancement of equatorial SST variance (fig. 5b).
359 These results collectively indicate that cloud feedbacks from the eastern subtropical
360 Atlantic can play an important role in setting the timescale and amplitude of equatorial modes of
361 variability especially at low-frequency timescales. It is of interest to understand if equatorial
362 SSTs are influenced by other regions in the South Atlantic or the Namibian region plays a unique
363 role in modulating equatorial Atlantic climate variability.
364

c. Role of cloud feedbacks over the other regions in the South Atlantic

To test the possible role of other regions in the South Atlantic, we perform nine experiments in which we increase the strength of positive cloud feedback over the nine boxes shown in fig. 1. We note that while in the Namib region cloud liquid water is mostly present at lower levels in the atmosphere (below 700hPa), in the other regions over the South Atlantic it can be present also at upper levels, especially where deep-convective clouds are predominant along the equator and the South Atlantic Convergence Zone. This means that in these nine experiments we are not influencing only low-level cloud feedbacks, although differently from observations cloud feedback over the deep-convective regions in the model (fig. 4b) has a net positive sign like over the Namibia region. Despite these differences from observations, these experiments will reveal the regions over the tropical South Atlantic where the positive feedback between cloud cover and SST can trigger a response over the equatorial Atlantic.

Figure 8 shows the difference in cloud feedback between the nine enhanced cloud feedback experiments and the control simulation. Cloud feedback is estimated as in fig. 4 as the regression of local CRE at the surface on local SST. Although we enhance positive cloud feedback in the same manner in all regions, we see from fig. 8 that regions where low-clouds are more common over the eastern Atlantic (e.g., Box 6 over the Namibian region) display a more enhanced positive cloud feedback. This is because the total cloud cover is larger where low-level clouds predominate.

The response to enhanced feedbacks is not trivially proportional to the change in cloud feedback strength shown in fig. 8. Figure 9 shows the ratio of SST variance in the nine cloud feedback experiments to the control simulation and there is not clear correspondence between enhanced cloud feedback (fig. 8) and SST variance (fig. 9). This is even more evident in fig. 10,

388 which shows the difference in cloud feedback from fig. 8 (green bars) versus the ratio of SST
389 variance (orange bars) averaged over the nine boxes in each corresponding experiments (i.e., the
390 bars for "Box 1" represent the averages over the coordinates of Box 1 in the Box 1 experiment,
391 etc.). For example, the variance of SST over Box 2 increases as much as over Box 1, but the
392 increase in cloud feedback over Box 2 is much bigger than over Box 1.

393 In general, we find that the effects of enhanced cloud feedbacks in the western Atlantic
394 (Boxes 1,4, and 7) and central equatorial Atlantic (Box 2) are small, whereas the central South
395 Atlantic (Boxes 5 and 8) and the eastern Atlantic (Boxes 3, 6, and 9) have more noticeable
396 impacts (see fig. 9). Box 6, which sits on the Namibian stratocumulus deck, has the largest
397 impact on the variance of local and equatorial SST. The effectiveness of the cloud-SST coupling
398 in this region highlights the importance of Namibian stratocumulus clouds in tropical Atlantic
399 variability and is consistent with the results of the Namib experiment. Box 3, which is located at
400 the eastern side of the equatorial Atlantic, also shows some influence on equatorial SST variance.

401 Although cloud feedbacks over Boxes 5 and 8 located over the central part of the basin
402 enhance local SST variance, they do not impact equatorial variability. Also of interest is that
403 cloud feedbacks over Box 2 and Box 3 not only increase SST variance along the equator, but
404 also over the central southern Atlantic (fig. 9). The connection between equatorial and the central
405 southern Atlantic is in contrast with the effects of cloud feedback over Box 8, which shows no
406 remote influence on SST variance along the equator.

407 In regards to the effects of these regional cloud feedbacks on the persistence of SST
408 anomalies, the difference in *e*-folding timescale between the nine experiments and the control
409 simulation in fig. 11 shows very little influence of cloud feedbacks from all regions with the
410 exception of Box 6 (Namibian region) and Box 3 (eastern equatorial Atlantic), although the

411 effects of Box 3 are much smaller. We note that positive cloud feedbacks over some regions on
412 the western side of the Atlantic actually tend to reduce the persistence of SST anomalies along
413 the eastern equatorial Atlantic (Boxes 1, 2, and 7 in fig. 10), but these effects are smaller.
414 The prominent role of positive cloud feedbacks over the Namibian region (Box 6)
415 compared to the equatorial eastern Atlantic (Box 3) is most clearly seen from power spectra of
416 SST anomalies of the Atl3 index computed for the nine regional experiments (fig. 12). Compared
417 to the control simulation (black), the only box that clearly enhances the variance of SST at inter-
418 annual and longer timescales is Box 6 (magenta). Since the difference in *e*-folding timescale
419 shown in fig. 11 indicates that also Box 3 over the eastern equatorial Atlantic exerts an influence
420 on the persistence of SST anomalies, we ran Box 3 and Box 6 for additional 50 years to ensure
421 that the effects of cloud feedback over Box 6 are not due to the length of the simulation. These
422 longer simulations are represented by lines with dot markers in fig. 12. The longer timeseries
423 show no effects on Atl3 SST anomalies from Box 3 (dotted orange line), while the effects from
424 Box 6 (dotted magenta line) become even more evident with a longer simulation, especially at
425 low-frequency timescales. For reference, we plot the power spectra for the Namib experiment for
426 80 years of simulation (solid gray line) and the full simulation (180 years; dotted gray line). The
427 Namib experiment increases the variance of equatorial SST anomalies by even more than Box 6.
428 Consistently with the values of *e*-folding timescale in fig. 11, the boxes over the western Atlantic
429 reduce the variance of the Atl3 index.
430 We verify that Box 6 has not the largest impact on SST variance just because enhanced
431 cloud feedback is larger than over the other boxes (fig. 8 and 10). We run an additional
432 experiment in which we make cloud feedback over Box 6 less sensitive to SST (referred to as

433 "Box 6b"). In this experiment, we change the relationship between cloud liquid water and SST
434 anomaly in eq. (1) to:

435 $$y = 1 - 0.7 * \arctan(0.7 * \mathrm{SST}) * 2/\pi \quad (3)$$

436 Although the overall increase in variance is less than that shown by Box 6 (see corresponding
437 bars in fig. 10), Box 6b still exhibits a large response at the equator especially at lower
438 frequencies, which is different from all the other boxes (see the Box 6b curve in the power
439 spectra of fig. 12).

440 In separate experiments, we enhanced the strength of cloud feedback according to eq. (1)
441 in the entire North Atlantic basin and over the North Atlantic subtropical stratocumulus region
442 (Canaries). These experiments show that enhanced cloud feedbacks over the North Atlantic
443 influence SST variability in the North Atlantic basin, but have no effects on equatorial Atlantic
444 variability.

445 Overall, model and observational analysis suggest that the Namibian region plays a
446 fundamental role on local and equatorial SST variability. Since we also verify that the central
447 role of the Namibian region on equatorial SSTs is not trivially related to (1) the fact that the
448 enhancement of cloud feedback is most effective over the Namibian region (fig. 8) or (2) the
449 length of the simulation (fig. 12), we now investigate in further detail the mechanisms of Atlantic
450 Niño variability in our slab-ocean simulations and the role of the Namibian region.

451

452 *c. The relationship between the Namibian region and equatorial Atlantic variability*

453 To understand why low-level cloud feedbacks over the Namibian region have a remote
454 influence along the equator, we compare the mean state of (shaded) SST, (contours) SLP, and
455 (vectors) winds in the control run (fig. 13) with lagged composites of these same variables during

warm events of the Atl3 SST index in the Namib experiment (fig. 14). Warm events are chosen as the months at which SST anomalies averaged over the Atl3 region exceed one standard deviation of the Atl3 index timeseries. We show the Namib experiment because anomalies are larger, but results are consistent if we use the control simulation. We obtain qualitatively similar results if we increase the threshold for warm events from 1.0 to 1.5 standard deviations or we look at cold instead of warm events.

In the mean state, the South Atlantic climate (fig. 13) is characterized by east-west and north-south gradients of SST with relatively colder SSTs where Namibian stratocumulus clouds are located. Mean surface winds are southeasterly over the Namibian region and easterly along the equator, and there is a counter-clockwise circulation at 30ºS associated with the subtropical high.

Lagged composites of Atl3 index warm events (fig. 14) show that anomalous warm SSTs develop over the southeast Atlantic at approximately 20ºS at lag -18 months from the peak of the warm events along with a weakening of the atmospheric circulation in the central part of the basin (fig. 14a). SSTs remain anomalously warm over the southeast Atlantic throughout the development of the event, while the reduced latent heat fluxes caused by the weakening of the trade winds favor the progressive warming of SSTs over the northeastern part of the basin through the WES feedback, until the Atl3 region (black box) reaches its warm peak. Differently from other regions, the trade winds over the eastern part of the South Atlantic (Namibian region) are regularly upwind of the equatorial regions, which is important for the WES feedback to work (cf. Klein et al. 1995).

The southwestern part of the basin that is characterized by opposite sign, cold SST anomaly, is driven by different but complementary mechanisms. If we compare this region with

479 the mean climate in fig. 13, we see a strengthening rather than a weakening of the surface winds.
480 The strengthening of the surface winds through latent heat fluxes, and the advection of cold air
481 from the southern mid-latitudes, promote colder SSTs in the southwest part of the basin.

482 The analysis of composites of the control simulation shows qualitatively similar results to
483 those shown in fig. 14 for the Namib experiment. The differences between the two simulations
484 are in the persistence of the events (cf. fig. 6), with the control simulation showing the first SST
485 anomalies over the southeast Atlantic at lag -12 instead of lag -18, and the magnitude of the
486 events, with the control simulation exhibiting weaker SST anomalies.

487 It is noteworthy that the mechanisms of the simulated Atlantic Niño in the slab-ocean
488 simulations are similar to observations. The composites of SST and atmospheric circulation on
489 the Atl3 index at lag 0 (fig. 14d) resemble the observed anomalies associated with Atlantic Niño
490 (fig. 2) although ocean dynamics are absent in our simulations (cf. Trzaska et al. 2007). In fact,
491 composites of the same fields in observations give similar results as in fig. 14 (not shown).
492 Therefore, understanding the dynamics of slab-ocean Atlantic Niño and the role of cloud
493 feedbacks is relevant to understand the processes driving Atlantic Niño and its persistence in the
494 real world (cf. Dommenget et al. 2014).

495

496 *e. Analysis of surface flux damping rates*

497 The variability of SST anomalies associated with Atlantic Niño can be explained using the
498 Frankignoul and Hasselmann (1977) framework, according to which the persistence of SST
499 anomalies is tied to the damping rate (λ) of SST:

500 $$\rho C_p H \frac{dT}{dt} = -\lambda T + N \quad (4)$$

where T is the temperature of the mixed layer (i.e., SST), H is the depth of the mixed layer, ρ is the density of seawater, and C_p is the specific heat of seawater at constant pressure. The term N is interpreted as stochastic noise from atmospheric weather that is integrated by the oceanic mixed layer. According to eq. (4), the persistence of SST is largest where the damping rate λ is weakest and the depth of the mixed layer H is greatest. In our experiments H does not change, therefore it does not influence the persistence of SST.

The damping rates can be linearly decomposed into contributions from each surface flux terms. Positive damping rates reduce the persistence of SST anomalies, while negative damping rates increase their persistence (cf. eq. 4). We calculate the damping rates as in Park et al. (2005):

$$\lambda_i = \frac{cov[Q_i(-L), SST(0)]}{cov[SST(-L), SST(0)]} \qquad (5)$$

where λ_i is the damping rate of each of the four surface fluxes Q_i (clear-sky radiation, CRE, latent heat, sensible heat), while "-L" indicates negative lags. In the equation, "*cov*" stands for covariance. Each λ_i is computed as the average of the first three negative lags (-1, -2, and -3 months).

Figure 15b shows that the sum of damping rates of the four surface fluxes is positive, that is, the fluxes tend to restore SST anomalies to their climatological mean. Of the four surface fluxes, the largest contribution to positive values comes from the latent heat flux (contours in fig. 15b), while the damping rate due to CRE is negative because cloud feedbacks tend to increase the persistence of SST anomalies over the eastern part of the basin (not shown). The damping rates associated with sensible heat and clear-sky radiation are one order of magnitude smaller.

The sign of the surface flux damping rates in the model is consistent with the observational estimates of Park et al. (2005), while the meridional structure of the damping rate is similar to the one estimated by Evan et al. (2013) (their fig. 5). The spatial pattern of the

damping rate in fig. 15b is consistent with the equatorial expansion of SST anomalies seen from the lagged composites (fig. 14). In fact, damping rates are weakest along the eastern part of the basin, hence with large-scale weakening of the trade winds, SST anomalies are the same sign and maximum in amplitude over the Namibian and eastern equatorial regions. Instead, the stronger damping rates over Box 1, 2, 4, and 7 explain why the variance of SST (fig. 9) does not increase as much as it does in the eastern part of the basin.

It is important to note that the SST anomalies associated with Atlantic Niño develop at lag -18 months where the variance of SST is largest (fig. 14), which occurs over the Namibian region (fig. 15d), and not at the equator, even though we composite by Atl3 SST anomalies. Also in the control simulation the peak of the composites (lag 0) occurs where the variance is largest in the control simulation, and not in the Atl3 region. In the slab-ocean experiments the variance of SST (fig 15d) can be explained to the first order as the variance of total surface fluxes (fig. 15a) scaled by the sum of the damping rates of these fluxes (fig. 15b). In fact, fig. 15c shows the variance of total fluxes divided by their total damping rate, which exhibits a spatial pattern that largely resembles the variance of SST (fig. 15d). When we enhance cloud feedback over Box 6 (black box) or the Namibian region (red box), we introduce a positive feedback that increases the variance of total surface flux and decreases its damping rate (not shown), and therefore increases the variance of SST. Box 6 has a smaller effect than the Namib experiment on equatorial SST spectra (fig. 12) because the Namib experiment encompasses a bigger region than Box 6 (see boxes in fig. 15d) where SST variance is large and damping rate is small.

In summary, SST anomalies associated with Atlantic Niño develop where the variance of SST is largest and the damping rate of SST is weakest, that is, over the Namibian region. This region is also upwind of the equatorial region regularly, while other regions in the South Atlantic

546 are not upwind as often (Klein et al. 1995). This explains why the Namibian subtropical
547 stratocumulus area is the most important region in affecting equatorial climate variability and the
548 slab-ocean Atlantic Niño.
549

550 4. Summary

551 Previous studies have shown the importance of stratocumulus clouds over the Namibian region
552 in enhancing meridional coupled modes of variability both in observations and theoretical
553 models (e.g.; Tanimoto and Xie 2002; Evan et al. 2013). For example, Evan et al. (2013)
554 showed that in the absence of cloud feedbacks over the stratocumulus regions the magnitude of
555 the WES feedback associated with meridionally propagating modes would not be sufficient to
556 overcome the damping rates of SST anomalies. Moreover, Klein et al. (1995) showed in
557 observations that stratocumulus clouds respond to upstream SST anomalies enhancing the WES
558 feedback and the propagation of SST anomalies. Here we build on these previous studies by
559 examining the role of cloud feedbacks in a full AGCM, and focusing on the role of cloud
560 feedbacks on equatorial Atlantic variability.

561 We examine observations of cloud radiative effect and show that Atlantic Niño SST
562 anomalies co-vary with positive cloud feedback over the Namibian stratocumulus region.
563 Changes in cloud cover seen in observations over this region can influence the persistence of
564 SST anomalies (e.g.; Park et al. 2005), but from observations alone it is not possible to
565 distinguish the role of regional cloud feedbacks on large-scale climate variability from other
566 processes.

567 To address this question, we perform sensitivity experiments using the atmospheric
568 component (ECHAM6) of an earth system model coupled to a slab-ocean, in which we

569 artificially increase the strength of positive cloud feedback over selected regions using the
570 experimental design of Bellomo et al. (2014b). We show that low-level cloud feedback over the
571 Namibian stratocumulus region influences the variance and persistence of large-scale SST
572 variability. In particular, low-level cloud feedback over the Namibian region enhances the
573 simulated Atlantic Niño in the model. Together, model and observations suggest that cloud
574 feedbacks can modify the characteristics and persistence of Atlantic Niño events.

575 We perform additional experiments to investigate the influence of cloud feedback in nine
576 regions spanning the tropical South Atlantic (5ºN-30ºS, 40ºW-10ºE). The purpose of these
577 experiments is to determine whether other regions influence local or remote SST variability. We
578 find that: regions over the central and eastern South Atlantic south of 20ºS increase only local
579 SST variability; regions over the eastern South Atlantic north of 20ºS increase both local and
580 equatorial SST variability; while regions over the western South Atlantic do not influence local
581 SST variability but they reduce equatorial SST variability, although their effects are small
582 compared to the eastern regions. Of all the regions, the Namibian stratocumulus region has the
583 strongest influence on the variance and persistence of equatorial Atlantic SSTs at inter-annual
584 and longer timescale.

585 We investigate the mechanisms associated with the development of Atlantic Niño events
586 using composites and regression analysis. We find that SST anomalies originating over the
587 Namibian region are amplified by positive cloud feedbacks. These anomalies eventually favor
588 anomalies of the same sign over the equatorial eastern Atlantic because they influence the
589 strength of surface winds and associated latent heat fluxes through the WES feedback. The
590 Namibian region has the largest impact of all the South Atlantic regions on the persistence of

591 equatorial SST anomalies because it is located where Atlantic Niño events develop, that is,
592 where the variance of SST is largest and the damping rate of SST is weakest.

593 Our approach is helpful to evaluate the effects of regional cloud-SST feedbacks on large-
594 scale modes of variability. However, we note that the variability of cloud cover and its effects on
595 SSTs is certainly influenced by other processes, including: inversion strength, subsidence rate,
596 radiative cooling above the boundary layer, and moisture above the inversion (e.g., Wood 2012),
597 which we have not examined here. We also have not addressed the role of ocean dynamics here
598 since our results are based on observations and experiments with an AGCM coupled to slab-
599 ocean. Power spectra of Atl3 index in CMIP3 models coupled to slab-ocean and full-ocean
600 models reveal that ocean dynamics enhance interannual variability with negligible effects at
601 longer timescales (not shown), consistently with the results of Clement et al. (2011) for Pacific
602 El Niño variability. Another study by Zhang et al. (2010) suggests that cloud feedbacks amplify
603 the large-scale effects induced by changes in the Atlantic Meridional Overturning Circulation
604 (AMOC). Hence, the interaction of cloud feedbacks with ocean dynamics remains an interesting
605 yet unresolved question.

606 Although we did not focus in this study on predictive skill, we note that predictability
607 increases if a timeseries of SSTs is strongly autocorrelated (i.e, if to predict the SST of next
608 month we assume that it will be the same as the present month scaled by the autocorrelation
609 function of SST). Since increasing the strength of positive cloud feedback results in a more
610 autocorrelated SST timeseries (as measured by the *e*-folding time), we expect that improving the
611 simulation of cloud processes and the coupling between clouds, SST, and circulations (Evan et
612 al. 2013; Stevens and Bony 2013) would lead to improved predictability of internal climate
613 variability.

Acknowledgements

We thank Paquita Zuidema and Nathan Laxague for helpful comments, and Amato Evan and two anonymous reviewers for insightful revisions. This work is supported by the Office of Science, U.S. DOE (grant #DESC0004897), NSF Climate and Large-scale Dynamics Program (grant #AGS0946225), NOAA climate program office (grant #NA10OAR4310204), the Rosenstiel Alumni Fellowship (2012), and by the Federal Ministry for Education and Research in Germany (BMBF) through the research program "MiKlip" (FKZ:01LP1158A).

References

Barreiro, M., A. Giannini, P. Chang, and R. Saravannan, 2004: On the role of the South Atlantic atmospheric circulation in tropical Atlantic variability. *Earth's Climate: The Ocean- Atmosphere Interaction*, Geophys. Monogr., Vol. 147, Amer. Geophys. Union, 143–156.

Bellomo, K., A. C. Clement, J. R. Norris, B. J. Soden, 2014a: Observational and Model Estimates of Cloud Amount Feedback over the Indian and Pacific Oceans. *J. Climate*, **27**, 925–940.

Bellomo K., A. C. Clement, T. Mauritsen, G. Rädel, and B. Stevens, in press. *J. Climate* (2014b): Simulating the role of subtropical stratocumulus clouds in driving Pacific climate variability

Biasutti, M., D. S. Battisti, and E. S. Sarachik, 2003: The annual cycle over the tropical Atlantic South America, and Africa, *J. Climate*, **16**, 2491-2508.

Boyer, D. C., C. H. Kirchner, M. K. McAllister, A. Staby, and B. I. Staalesen, 2001: The orange roughy fishery of Namibia: Lessons to be learned about managing a developing fishery. Pp. 205-211 In: Paine, A. I. L., Pillar, S. C. and Crawford, R. J. M. (eds.). A decade of Namibian fisheries science. *South African Journal of Marine Science*, 23.

Brundrit, G. B., Trends of southern African sea level, 1995: Statistical analysis and interpretation, *S. Afr. J. Mar. Sci*., **16**, 9–17.

Carton, J. A., X. Cao, B. S. Giese, and A. M. da Silva, 1996: Decadal and interannual SST variability in the tropical Atlantic Ocean, *J. Phys. Oceanogr.*, **26**, 1165-1175.

Chang, P., L. Ji, and H. Li, 1997: A decadal climate variation in the tropical Atlantic Ocean from thermodynamic air–sea inter- actions. *Nature*, **385**, 516–518.

Chaves, R. R., and P. Nobre, 2004: Interactions between sea sur- face temperature over the South Atlantic Ocean and the South Atlantic convergence zone. *Geophys. Res. Lett.*, **31**, L03204, doi:10.1029/2003GL018647.

Chiang, J. C. H., and D. J. Vimont, 2004: Analogous Pacific and Atlantic meridional modes of tropical atmosphere–ocean variability. *J. Climate*, **17**, 4143–4158.

Clement, A. C., P. DiNezio, and C. Deser, 2011: Rethinking the ocean's role in the Southern Oscillation. *J. Climate*, **24**, 4056–4072.

Clement, A. C., R. Burgman, and J. Norris, 2009: Model and observational evidence for positive low-level cloud feedback. *Science*, **325**, 460–464, doi:10.1126/science.1171255.

Delecluse, P., J. Servain, C. Levy, K. Arpe, and L. Bengtsson, 1994: On the connection between the 1984 Atlantic warm event and the 1982–83 ENSO. *Tellus*, **46A**, 448–464.

Dommenget, D., 2010: A slab ocean El Nino. *Geophys. Res. Lett.*,**37**, L20701, doi:10.1029/2010GL044888.

Dommenget, D., and M. Latif, 2000: Interannual to decadal variability in the tropical Atlantic. *J. Climate*, **13**, 777–792.

Dommenget, D., S. Haase, T. Bayr and C. Frauen, 2014: Analysis of the Slab-Ocean El Niño Atmospheric Feedbacks in Observed and Simulated ENSO Dynamics, *Climate Dyn*., http://dx.doi.org/10.1007/s00382-014-2057-0

Enfield, D. B., A. M. Mestas-Nunez, D. A. Mayer, and L. Cid- Serrano, 1999: How ubiquitous is the dipole relationship in tropical Atlantic sea surface temperatures?, *J. Geophys. Res.*, **104**, 7841- 7848.

Eastman, R., S. G. Warren, and C. J. Hahn, 2011: Variations in cloud cover and cloud types over the Ocean from surface observations, 1954–2008. *J. Climate*, **24**, 5914–5934.

Evan, A. T., R. J. Allen, Vimont, D. J. and R. Bennartz, 2013: The Modification of Sea Surface Temperature Anomaly Linear Damping Time Scales by Stratocumulus Clouds. *J. Climate*, **26**, 3619–3630.

Florenchie, P., J. R. E. Lutjeharms, C. J. C. Reason, S. Masson, and M. Rouault, 2003: The source of Benguela Niños in the South Atlantic Ocean, *Geophys. Res. Lett.*, **30**(10), 1505, doi:10.1029/2003GL017172

Florenchie, P., C. J. C. Reason, J. R. E. Lutjeharms, M. Rouault, C. Roy, and S. Masson, 2004: Evolution of interannual warm and cold events in the southeast Atlantic Ocean. *J. Climate*, **17**, 2318–2334.

Frankignoul, C., and K. Hasselmann, 1977: Stochastic climate models. Part 2. Application to sea-surface temperature variability and thermocline variability. *Tellus*, **29**, 284–305.

Grodsky S. A., and J. A. Carton, 2003: Intertropical Convergence Zone in the South Atlantic and the equatorial cold tongue, *J. Climate*, **16**, 723-733.

Haarsma, R. J., E. J. D. Campos, and F. Molteni, 2003: Atmospheric response to South Atlantic SST dipole. *Geophys. Res.*
Lett., **30**, 1864, doi:10.1029/2003GL017829.

Hagen, E., R. Feistel, J. J. Agenbag, and T. Ohde, 2001: Seasonal and interannual changes in intense Benguela upwelling (1982–1999), *Oceanol. Acta*, **24**, 557-567.

Hahn, C. J. and S. G. Warren, 1999: Extended edited synoptic cloud reports from ships and land stations over the globe, 1952–1996. Carbon Dioxide Information Analysis Center Rep. CDIAC/ NDP-026C, doi:10.3334/CDIAC/cli.ndp026c.

Hahn, C. J. and S. G. Warren, 2009: Extended edited synoptic cloud reports from ships and land stations over the globe, 1952–1996 (2009 update). Carbon Dioxide Information Analysis Center Numerical Data Package NDP-026C, 79 pp, doi:10.3334/ CDIAC/cli.ndp026c.

Hirst, A., and S. Hastenrath, 1983: Atmosphere-ocean mechanisms of climate anomalies in the Angola-tropical Atlantic sector, *J. Phys.Oceanogr.*, **13**, 1146-1157.

Hisard, P., 1980: Observation de response du type "El Nino" dans l'Atlan-tique tropical oriental – Golfe de Guinee, *Oceanol. Acta*, **3**, 69-78.

Horel, J. D., V. E. Kousky, and M. T. Kagano, 1986: Atmospheric conditions in the Atlantic sector during 1983 and 1984, *Nature*, **310**, 248–251.

Houghton, R. W., and Y. M. Tourre, 1992: Characteristics of low-frequency sea surface temperature fluctuations in the tropical Atlantic. *J. Climate,* **5,** 765–771.

Kalnay, and Coauthors, 1996: The NCEP/NCAR 40-Year Re- analysis Project. *Bull. Amer. Meteor. Soc.*, **77**, 437–470.

Klein, S. A., and D. L. Hartmann, 1993: The seasonal cycle of low stratiform clouds. *J. Climate*, **6**, 1587–1606.

Klein, S. A., D. L. Hartmann, and J. R. Norris, 1995: On the relationships among low- cloud structure, sea surface temperature, and atmospheric circulation in the summertime northeast Pacific. *J. Climate*, **8**, 1140–1155.

Loeb, N. G., B. A. Wielicki, D. R. Doelling, G. L. Smith, D. F. Keyes, S. Kato, N. Manalo-Smith, and T. Wong, 2009: Toward optimal closure of the Earth's top-of-atmosphere radiation budget. *J. Climate*, **22**, 748-766.

Marshall J., and Coauthors, 2001: North Atlantic climate variability: Phenomena, impacts, and mechanisms. *Int. J. Climatol.*, **21**, 1863-1898.

Matei, D., N. Keenlyside, M. Latif, and J. Jungclaus, 2008: Sub- tropical forcing of tropical Pacific climate and decadal ENSO modulation. *J. Climate*, **21**, 4691–4709.

Medeiros, B., and B. Stevens, 2011: Revealing differences in GCM representations of low clouds. *Climate Dyn*., **36**, 385–399,doi:10.1007/s00382-009-0694-5

Mehta, V. M., 1998: Variability of the tropical ocean surface tem- perature at decadal-multidecadal time scales. Part I: Atlantic Ocean. *J. Climate,* **11,** 2351–2375.

Merle, J., 1980: Annual and interannual variability of temperature in the eastern equatorial Atlantic Ocean – hypothesis of an Atlantic El Nino, *Oceanol. Acta*, **3**, 209-220.

Mitchell, T. P., and J. M. Wallace, 1992: On the annual cycle in equatorial convection and sea surface temperature. *J. Climate*, **5**, 1140–1156.

Nobre, P., and J. Shukla, 1996: Variations of sea surface temperature, wind stress, and rainfall over the tropical Atlantic and South America. *J. Climate*, **9**, 2464-2479.

Norris, J. R., 2005: Multidecadal changes in near-global cloud cover and estimated cloud cover radiative forcing. *J. Geophys. Res*., **110**, D08206, doi:10.1029/2004JD005600

Okumura, Yuko M., 2013: Origins of Tropical Pacific Decadal Variability: Role of Stochastic Atmospheric Forcing from the South Pacific. *J. Climate*, **26**, 9791–9796.

Park, S., C. Deser, and M. A. Alexander, 2005: Estimation of the surface heat flux response to sea surface temperature anom- alies over the global oceans. *J. Climate*, **18**, 4582–4599.

Penland, C., and L. Matrosova, 1998: Prediction of tropical Atlantic sea surface temperatures using linear inverse modeling. *J. Climate,* **11,** 483–496.

Robertson, A.W., J. D. Farrara, and C. R. Mechoso, 2003: Simulations of the atmospheric response to South Atlantic sea surface tempera- ture anomalies. *J. Climate*, **16**, 2540–2551.

Rossow, W. B., and R. A. Schiffer, 1999: Advances in un- derstanding clouds from ISCCP. *Bull. Amer. Meteor. Soc.*, **80**, 2261–2287.

Ruiz-Barradas, A., J. A. Carton, and S. Nigam, 2000: Structure of interan- nual-to-decadal climate variability in the tropical Atlantic sector, *J. Climate*, **13**, 3285-3297.

Servain, J. M., 1991: Simple climatic indices for the tropical Atlantic Ocean and some application. *J. Geophys. Res.*, **96**, 15137-15146.

Servain J, and A. Dessier, 1999: Relationship between equatorial and meridional modes of climatic variability in the tropical Atlantic. *Geophys. Res. Lett.*, **26**, 485–488.

Servain, J., I. Wainer, J. P. McCreary, and A. Dessier, 1999: Relationships between the equatorial and meridional modes of climatic variability in the tropical Atlantic. *Geophys. Res. Lett.*, **26**, 485-488.

Smith, T. M., R. W. Reynolds, T. C. Peterson, and J. Lawrimore, 2008: Improvements to NOAA's historical merged land–ocean surface temperature analysis (1880–2006). *J. Climate*, **21**, 2283–2296.

Sterl, A., and W. Hazeleger, 2003: Coupled variability and air-sea interaction in the South Atlantic Ocean. *Climate Dyn.*, **21**, 559–571.

Stevens, B., and S. Bony, 2013: What are climate models missing?, *Science*, **340** (6136), 105-1054.

Stevens, B. and Coauthors, 2013: The Atmospheric Component of the MPI-M Earth System Model: ECHAM6. *J. Adv. Model Earth Syst.*, **5**, 146-172, doi:10.1002/jame.20015.

Sutton, R. T., S. P. Jewson, and D. P. Rowell, 2000: The elements of climate variability in the tropical Atlantic. *J. Climate*, **13**, 3261–3284.

Tanimoto, Y., and S.-P. Xie, 2002: Inter-hemispheric decadal variations in SST, surface wind, heat flux and cloud cover over the Atlantic Ocean, *J. Meteorol. Soc. Jpn.*, **80**, 1199-1219.

Taylor, K. E., R. J. Stouffer, and G. A. Meehl, 2012: An overview of CMIP5 and the experiment design. *Bull. Amer. Meteor. Soc.,* **93**, 485-498.

Trzaska, S., A. W. Robertson, J. D. Farrara, C. R. Mechoso, 2007: South Atlantic Variability Arising from Air–Sea Coupling: Local Mechanisms and Tropical–Subtropical Interactions. *J. Climate*, **20**, 3345–3365.

Venegas, S. A., L. A. Mysak, and D. N. Straub, 1996: Evidence for interannual and interdecadal climate variability in the South Atlantic. *Geophys. Res. Lett.*, **23**, 2673–2676.

Wagner, R. G., and A. da Silva, 1994: Surface conditions associated with anomalous rainfall in the Guinea coastal region, *Int. J. Climatol.*, **14**, 179-200.

Wood R., 2012: Stratocumulus clouds, *Mon. Wea. Rev.*, **140**, 2373-2423.

Xie, S.-P., and J. A. Carton, 2004: Tropical Atlantic variability:Patterns, mechanisms, and impacts. *Earth's Climate: The Ocean-Atmosphere Interaction, Geophys. Monogr.*, Vol. 147, Amer. Geophys. Union, 121–142.

Zebiak, S. E., 1993: Air-sea interaction in the equatorial Atlantic region, *J. Climate*, **6**, 1567-1586, 1993.

Zelinka, M. D., S. A. Klein, and D. L. Hartmann, 2012: Computing and partitioning cloud feedbacks using cloud property histograms. Part II: Attribution to changes in cloud amount, altitude, and optical depth. *J. Climate*, **25**, 3736–3754.

Zhang, H., A. Clement, and P. DiNezio, 2014a: The South Pacific meridional mode: A mechanism for ENSO-like variability, *J. Climate*, **27**, 769–783.

Zhang, H., C. Deser, A. Clement, and R. Tomas, 2014b: Equatorial signatures of the Pacific Meridional Modes: Dependence on mean climate state, *Geophys. Res. Lett.*, **41**, 568–574.

Zhang, R., S. M. Kang, and I. M. Held, 2010: Sensitivity of climate change induced by the weakening of the Atlantic meridional overturning circulation to cloud feedback. *J. Climate*, **23**, 378–389.

869 Zhou, Z., and J. A. Carton, 1998: Latent heat flux and interannual variability of the coupled
870 atmosphere–ocean system. *J. Atmos. Sci*., **55**, 494–501.
871
872
873
874
875
876
877
878
879
880
881
882
883
884
885
886
887

List of Figures

Figure 1. Masking used in the model experiments with enhanced positive cloud feedback. Red box: Namib experiment; black boxes 1-9: regional experiments in the South Atlantic.

Figure 2. Regression of observed (shaded) SST, (contours) SLP, (vectors) surface winds on the Atl3 SST index (black box) for the years 1960-2010. Contours are from -2.0 hPa to 2.0 hPa with interval of 0.2 hPa. Solid lines refer to positive SLP anomalies, dashed lines to negative SLP anomalies, while the thick solid line is the zero-level contour. Stippling indicates where the correlation between local SSTs and the Atl3 SST index is statistically significant at the 95% level of the Pearson's R-test for correlations. All data are de-trended.

Figure 3. Regressions on the Atl3 index (black box) of (shaded) cloud amount feedback, units of W m^2 K^{-1}; (contours) cloud cover, units of % K^{-1}. Contour levels range from -10% to +10%, with 1% interval. Solid lines indicate positive values, dashed lines indicate negative values, while solid thick lines indicate the zero-level. (a) Cloud cover is from ISCCP (years 1984-2007); (b) Cloud cover is from EECRA (years 1954-2008). In this plot we use inter-annual anomalies differently from all the other plots because the temporal resolution of EECRA is of seasonal monthly means.

Figure 4. (a) Difference in local cloud feedback between Namib and the control simulation. Cloud feedback is computed as regression of local CRE at the surface on SST (units of W m^{-2} K^{-1}). Contours represent mean cloud cover climatology in the control simulation. Black box represents the Namib region; (b) Cloud feedback in the control simulation; (c) Cloud feedback

using CRE at the surface from CERES (2001-2009); (d) Cloud feedback using CRE at the surface from ISCCP (1984-2007).

Figure 5. (a) Variance of SST in the control simulation; (b) Ratio of variance of SST in the Namib experiment to the control simulation; (c) Variance of SLP in the control simulation; (d) Ratio of variance of SLP in the Namib experiment to the control simulation. Stippling indicates where the difference in variance between the Namib and the control simulations is significant at the 95% level of a Fisher's F-test. The black box indicates the Namib region.

Figure 6. (a) *e*-folding timescale in the control simulation; (b) difference in *e*-folding timescale between the Namib and the control simulations. The black box indicates the Namib region.

Figure 7. Power spectra of SST averaged over the Atl3 region (5ºS-5ºN, 20ºW-0ºE) in the (red) Namib experiment and (black) control simulation. A 24-month smoothing has been applied to the periodogram estimates. Black dots indicate where the variance of the Namib curve is significantly different from the variance of the control simulation at the 95% level of a Fisher's F-test.

Figure 8. Difference in cloud feedback between enhanced cloud feedback experiments and the control simulation. Cloud feedback is estimated as regression of local CRE at the surface on SST, units of W m^{-2} K^{-1} (as in fig. 4). The black-boxed regions in each plot indicate where positive cloud feedback is enhanced.

Figure 9. Ratio of variance of SST in the nine enhanced cloud feedback experiments to the control simulation. Stippling indicates where the difference in variance between the enhanced

928 cloud feedback experiments and the control simulation is significant at the 85% level of a
929 Fisher's F-test.

930 **Figure 10.** Values of difference in cloud feedback from fig. 8 (green) and ratios of SST variance
931 from fig. 9 (orange) averaged over the nine boxes in each corresponding experiment. Units are
932 W m^{-2} K^{-1} for the differences in cloud feedback, while the ratios of SST variance are unitless.

933 **Figure 11.** Difference in *e*-folding timescale between the nine enhanced cloud feedback
934 experiments and the control simulation.

935 **Figure 12.** Power spectra of SST averaged over the Atl3 region (5ºS-5ºN, 20ºW-0ºE) in the
936 (black) control simulation and (colors) enhanced cloud feedback experiments (see legend). A 24-
937 month smoothing has been applied to the periodogram estimates. The power spectra are
938 computed on timeseries of 80 years with the exception of the lines with markers (see legend).

939 **Figure 13.** Mean climatology in the control simulation: (shaded) SST in ºC, (contours) SLP in
940 hPa, (vectors) surface winds in m s^{-1}.

941 **Figure 14.** Lagged composites of warm Atl3 index events in the Namib experiment: (shaded)
942 SST, units of ºC, (contours) SLP, units of hPa, ranging from -2 hPa to 2 hPa with intervals of 0.2
943 hPa, (vectors) surface winds, units of m s^{-1}. (a) Lag -18 months from the peak of the event; (b)
944 Lag -12; (c) Lag -6; (d) Lag 0. The white box highlights the Namib region, while the black box
945 highlights the Atl3 region.

946 **Figure 15.** (a) Variance of the sum of the net surface fluxes (long-wave + short-wave + latent +
947 sensible); (b) Damping rate of net surface fluxes computed as in Park et al. (2005); (c) Variance

of net surface fluxes divided by their damping rate; (d) Variance of SST in the control simulation (same as in fig. 5a). Superimposed are (red) box of the Namib experiment and the (black) box of the Box 6 experiment.

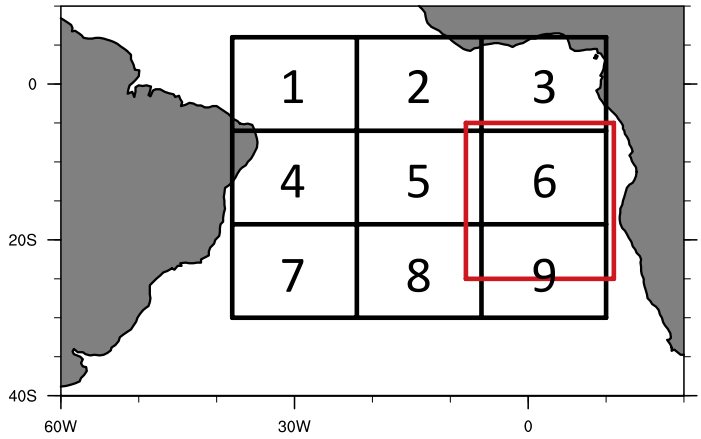

960

961 Figure 1. Masking used in the model experiments with enhanced positive cloud feedback. Red
962 box: Namib experiment; black boxes 1-9: regional experiments in the South Atlantic.

963

964

965

966

967

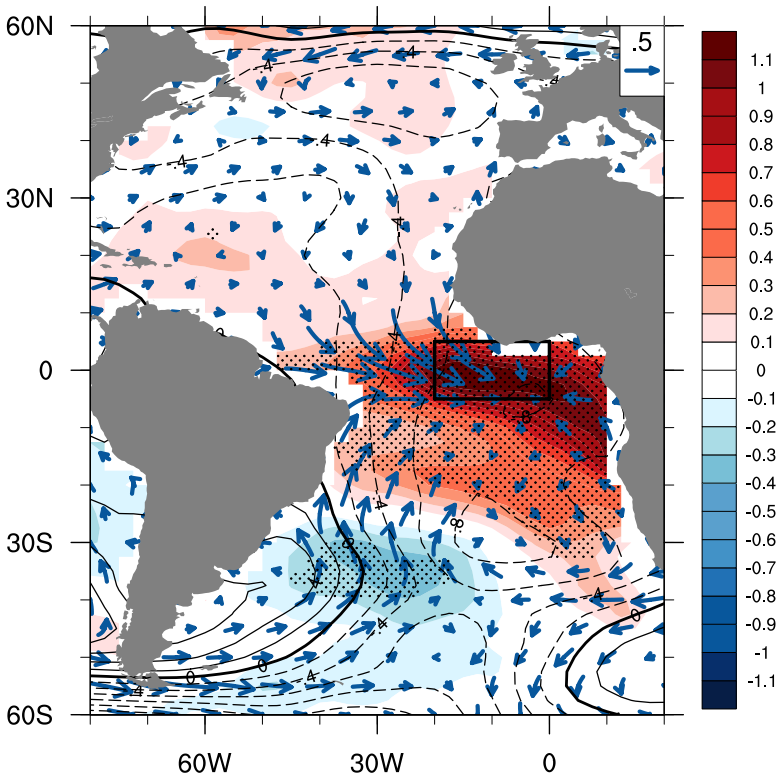

Figure 2. Regression of observed (shaded) SST, (contours) SLP, (vectors) surface winds on the Atl3 SST index (black box) for the years 1960-2010. Contours are from -2.0 hPa to 2.0 hPa with interval of 0.2 hPa. Solid lines refer to positive SLP anomalies, dashed lines to negative SLP anomalies, while the thick solid line is the zero-level contour. Stippling indicates where the correlation between local SSTs and the Atl3 SST index is statistically significant at the 95% level of the Pearson's R-test for correlations. All data are de-trended.

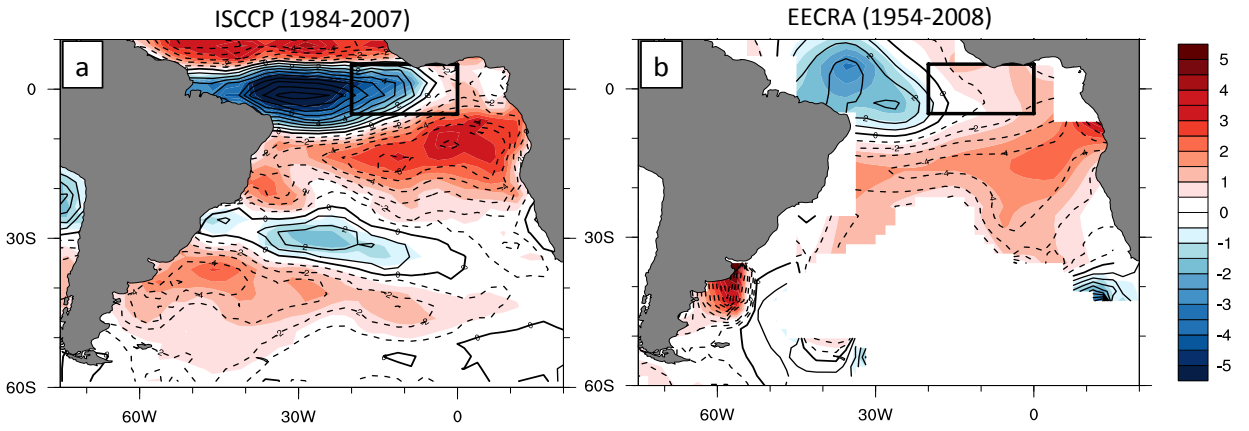

Figure 3. Regressions on the Atl3 index (black box) of (shaded) cloud amount feedback, units of W m^2 K^{-1}; (contours) cloud cover, units of % K^{-1}. Contour levels range from -10% to +10%, with 1% interval. Solid lines indicate positive values, dashed lines indicate negative values, while solid thick lines indicate the zero-level. (a) Cloud cover is from ISCCP (years 1984-2007); (b) Cloud cover is from EECRA (years 1954-2008). In this plot we use inter-annual anomalies differently from all the other plots because the temporal resolution of EECRA is of seasonal monthly means.

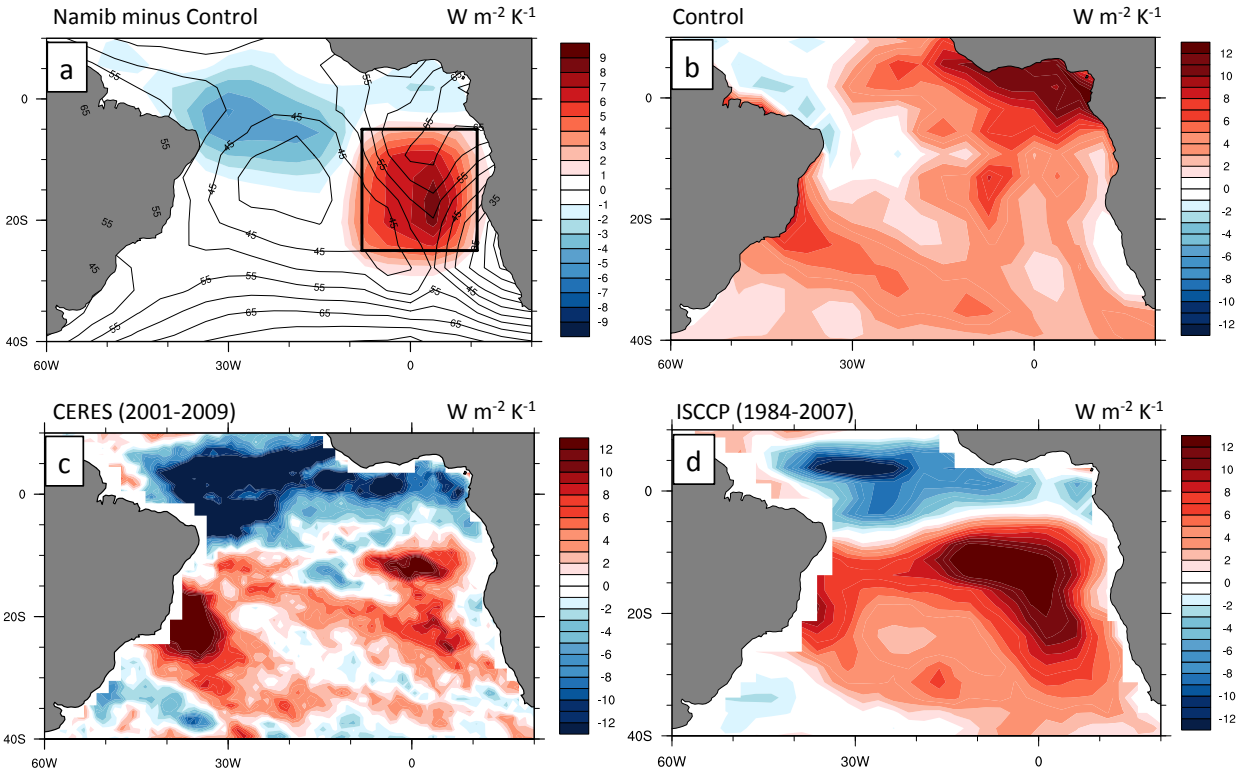

Figure 4. (a) Difference in local cloud feedback between Namib and the control simulation. Cloud feedback is computed as regression of local CRE at the surface on SST (units of W m^{-2} K^{-1}). Contours represent mean cloud cover climatology in the control simulation. Black box represents the Namib region; (b) Cloud feedback in the control simulation; (c) Cloud feedback using CRE at the surface from CERES (2001-2009); (d) Cloud feedback using CRE at the surface from ISCCP (1984-2007).

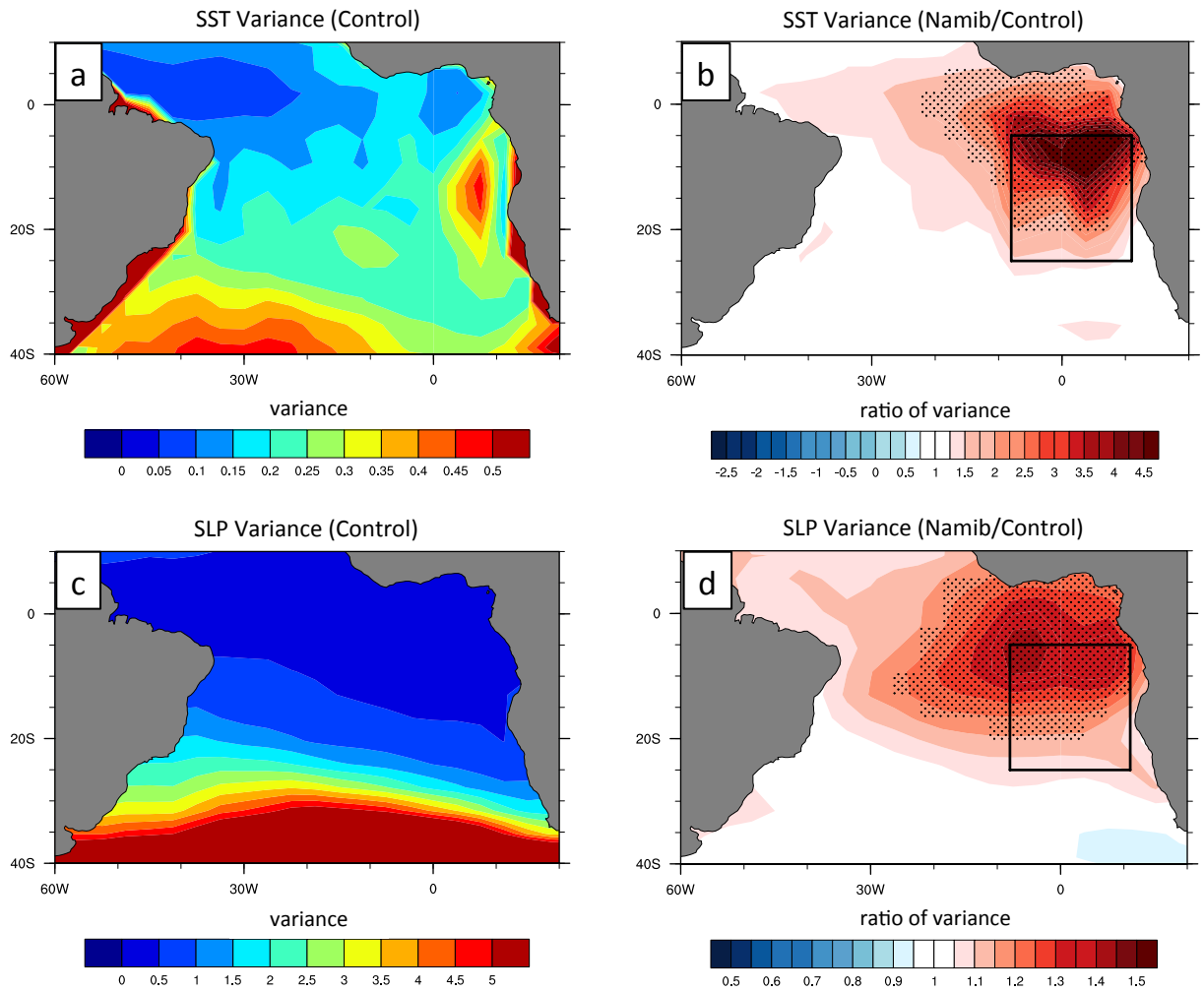

Figure 5. (a) Variance of SST in the control simulation; (b) Ratio of variance of SST in the Namib experiment to the control simulation; (c) Variance of SLP in the control simulation; (d) Ratio of variance of SLP in the Namib experiment to the control simulation. Stippling indicates where the difference in variance between the Namib and the control simulations is significant at the 95% level of a Fisher's F-test. The black box indicates the Namib region.

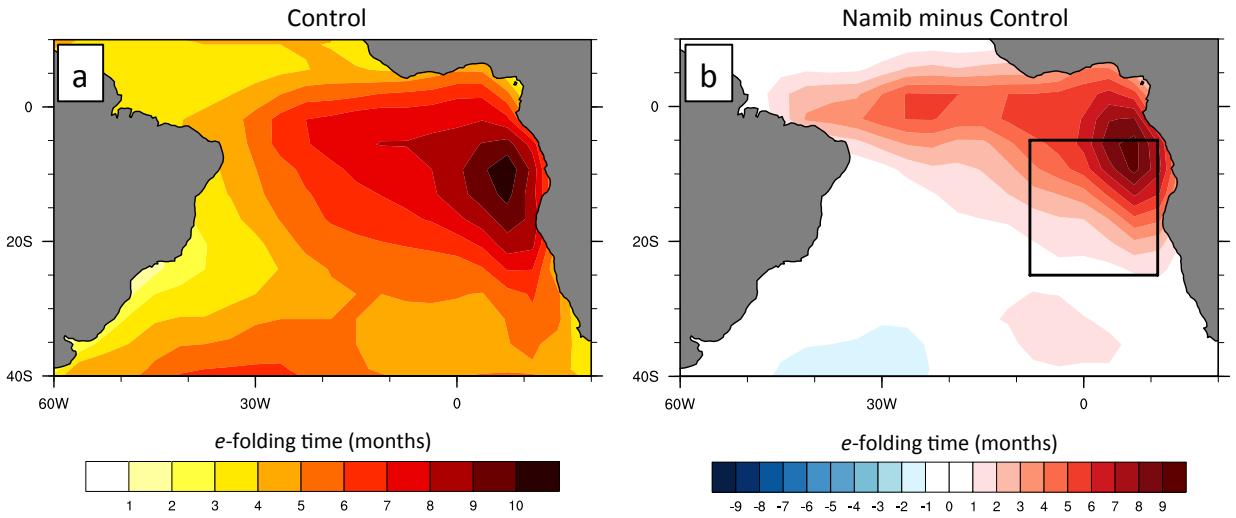

Figure 6. (a) *e*-folding timescale in the control simulation; (b) difference in *e*-folding timescale between the Namib and the control simulations. The black box indicates the Namib region.

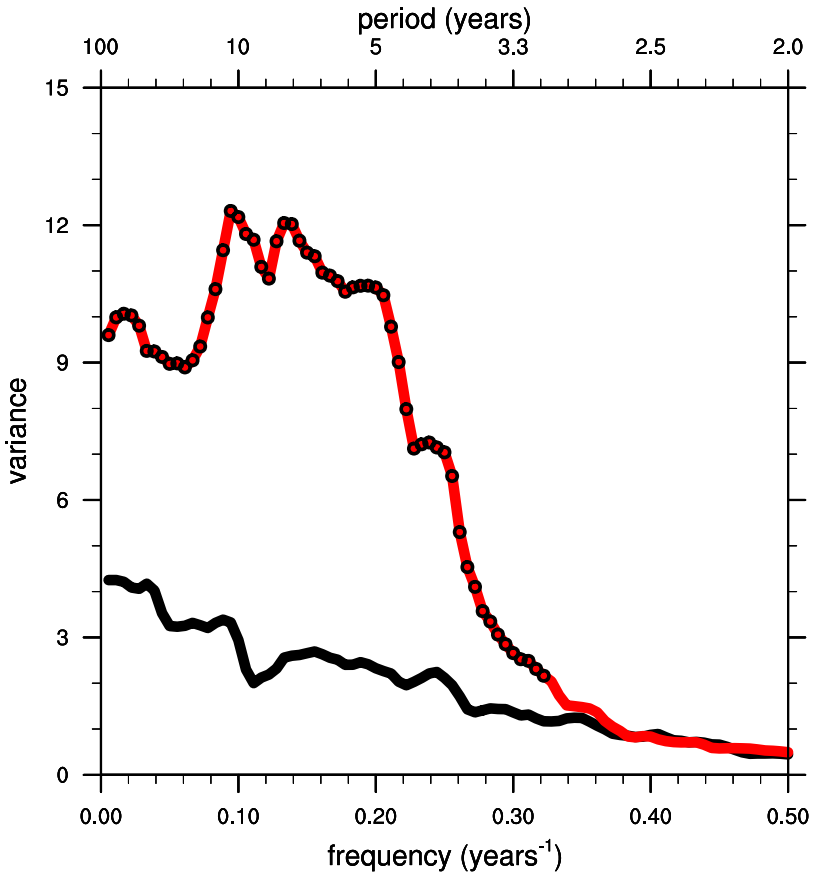

Figure 7. Power spectra of SST averaged over the Atl3 region (5ºS-5ºN, 20ºW-0ºE) in the (red) Namib experiment and (black) control simulation. A 24-month smoothing has been applied to the periodogram estimates. Black dots indicate where the variance of the Namib curve is significantly different from the variance of the control simulation at the 95% level of a Fisher's F-test.

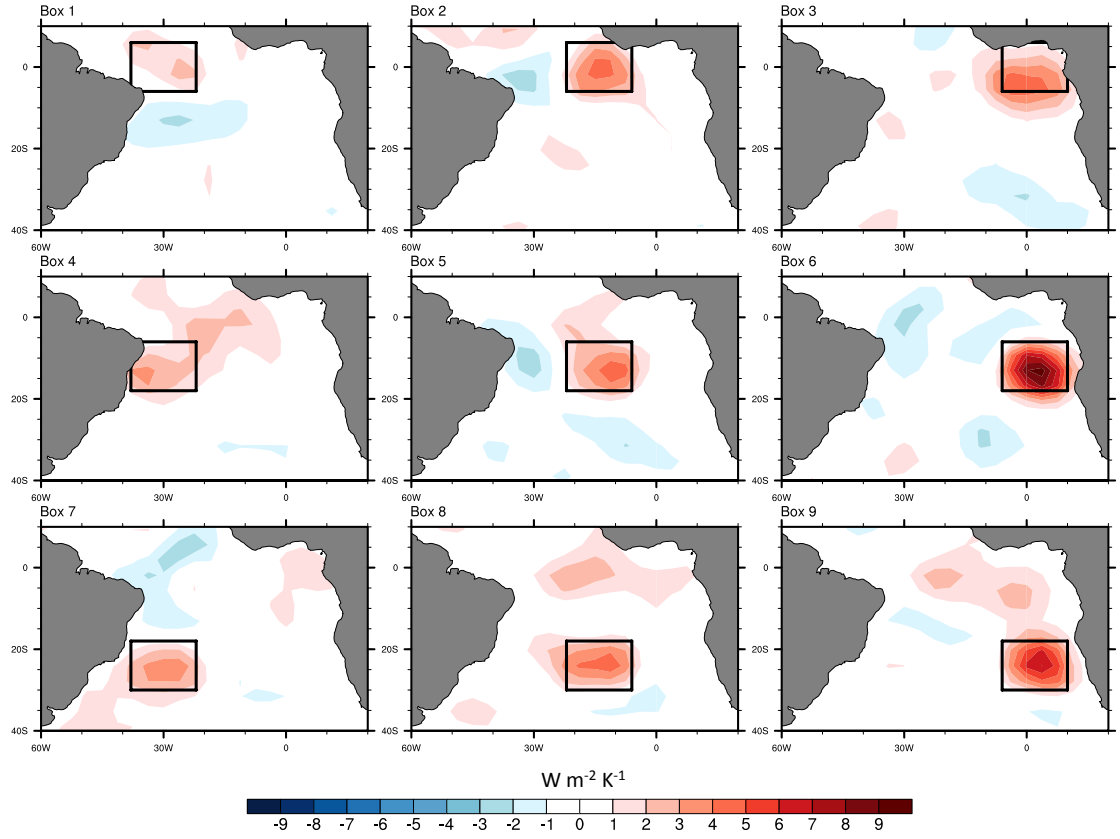

Figure 8. Difference in cloud feedback between enhanced cloud feedback experiments and the control simulation. Cloud feedback is estimated as regression of local CRE at the surface on SST, units of W m^{-2} K^{-1} (as in fig. 4). The black-boxed regions in each plot indicate where positive cloud feedback is enhanced.

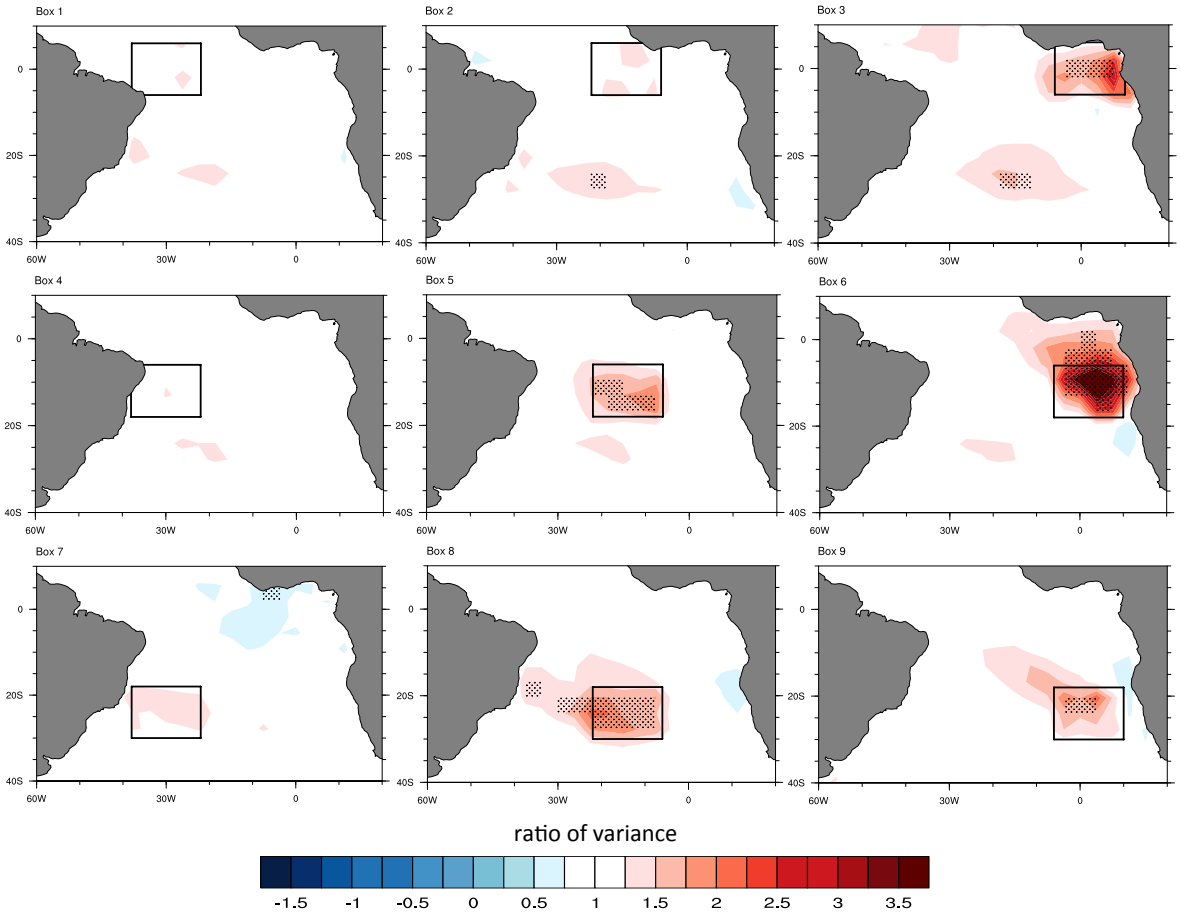

Figure 9. Ratio of variance of SST in the nine enhanced cloud feedback experiments to the control simulation. Stippling indicates where the difference in variance between the enhanced cloud feedback experiments and the control simulation is significant at the 85% level of a Fisher's F-test.

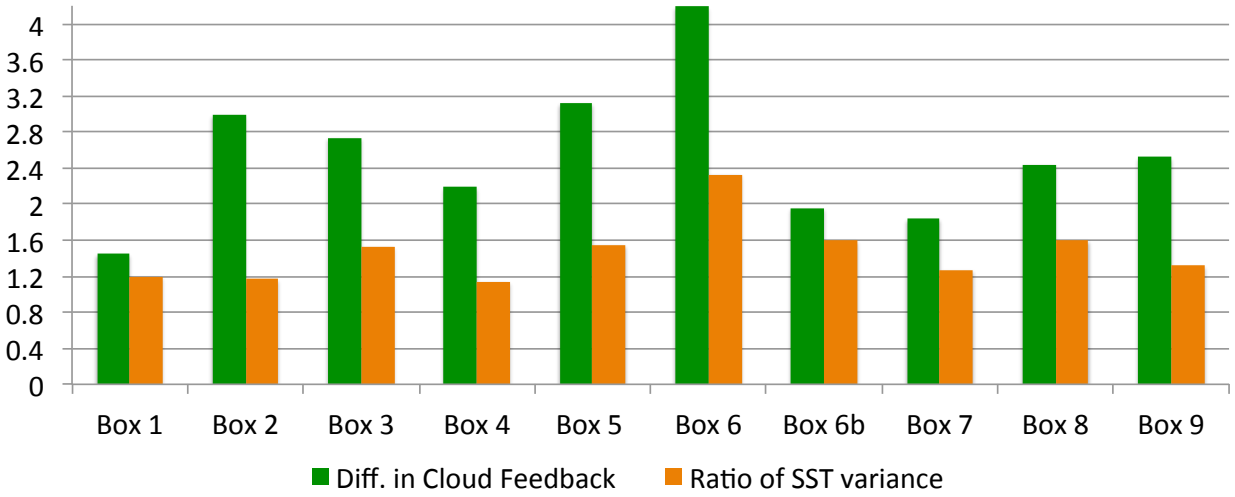

Figure 10. Values of difference in cloud feedback from fig. 8 (green) and ratios of SST variance from fig. 9 (orange) averaged over the nine boxes in each corresponding experiment. Units are W m^{-2} K^{-1} for the differences in cloud feedback, while the ratios of SST variance are unitless.

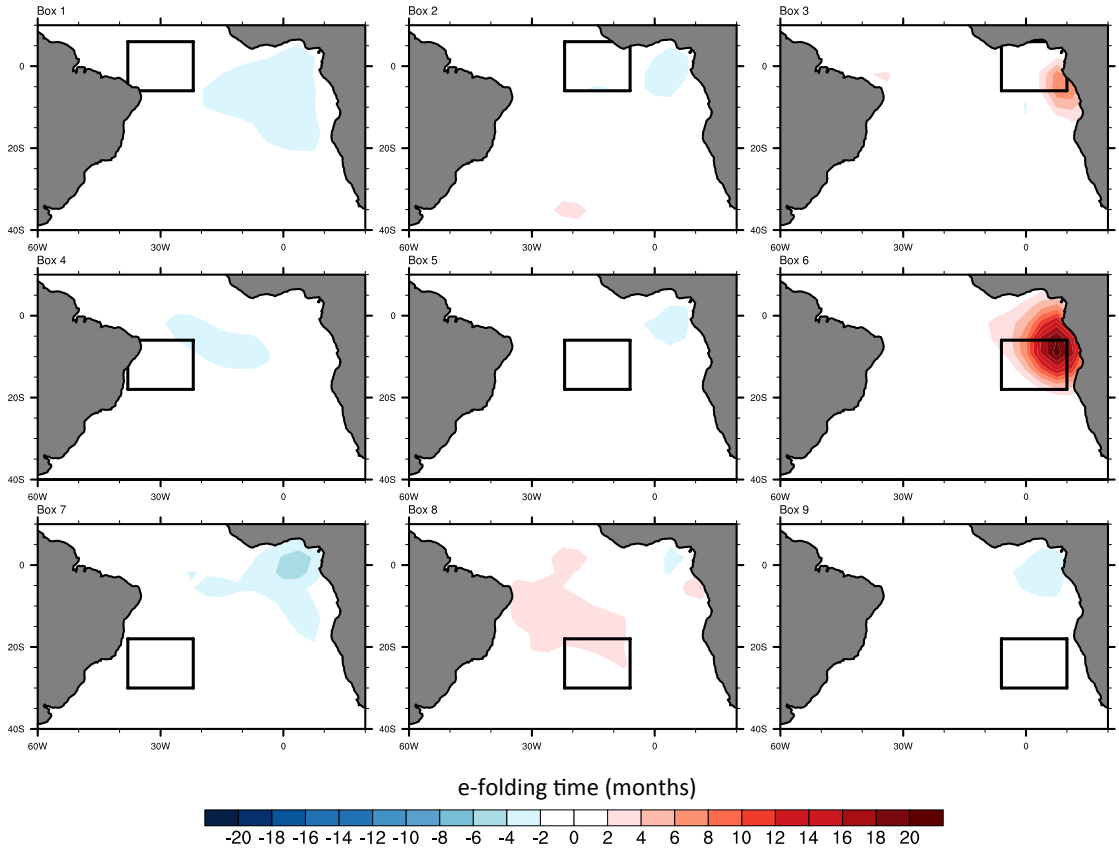

Figure 11. Difference in *e*-folding timescale between the nine enhanced cloud feedback experiments and the control simulation.

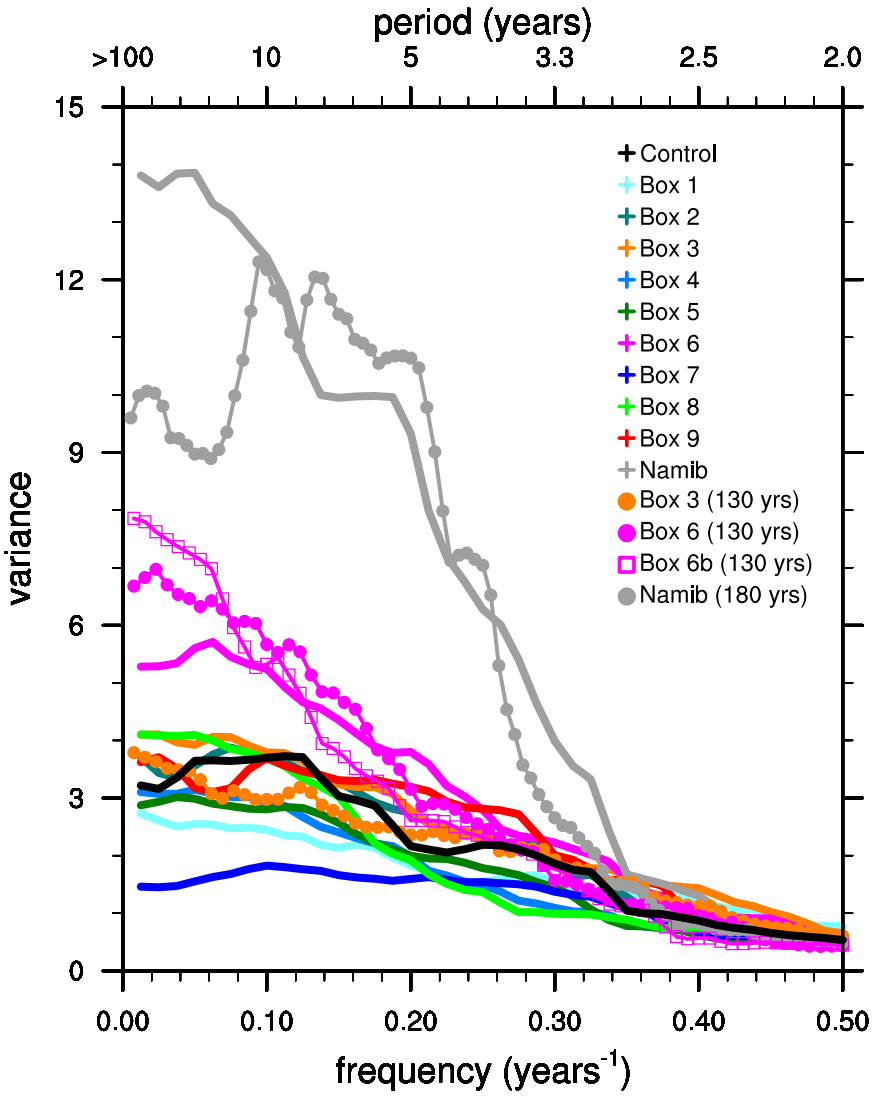

Figure 12. Power spectra of SST averaged over the Atl3 region (5ºS-5ºN, 20ºW-0ºE) in the (black) control simulation and (colors) enhanced cloud feedback experiments (see legend). A 24-month smoothing has been applied to the periodogram estimates. The power spectra are computed on timeseries of 80 years with the exception of the lines with markers (see legend).

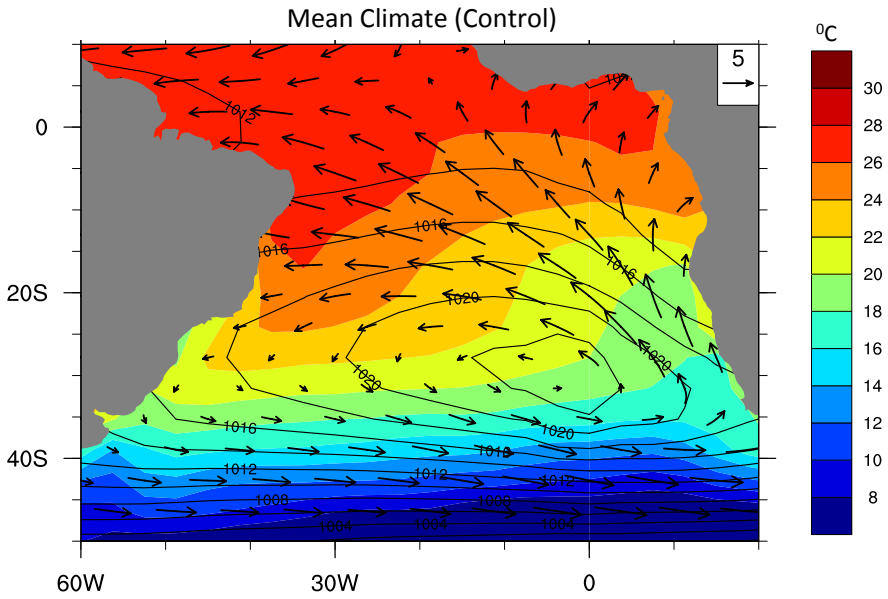

Figure 13. Mean climatology in the control simulation: (shaded) SST in ºC, (contours) SLP in hPa, (vectors) surface winds in m s^{-1}.

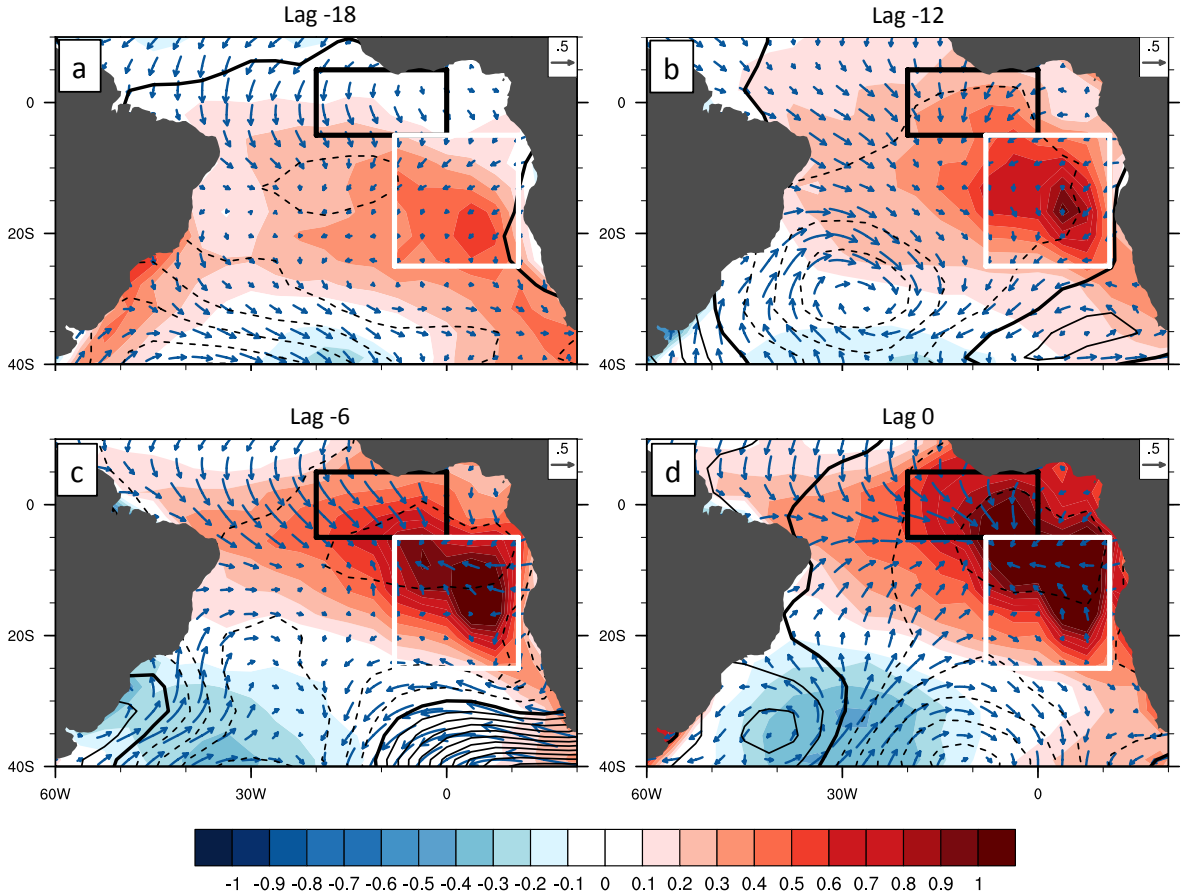

Figure 14. Lagged composites of warm Atl3 index events in the Namib experiment: (shaded) SST, units of ºC, (contours) SLP, units of hPa, ranging from -2 hPa to 2 hPa with intervals of 0.2 hPa, (vectors) surface winds, units of m s^{-1}. (a) Lag -18 months from the peak of the event; (b) Lag -12; (c) Lag -6; (d) Lag 0. The white box highlights the Namib region, while the black box highlights the Atl3 region.

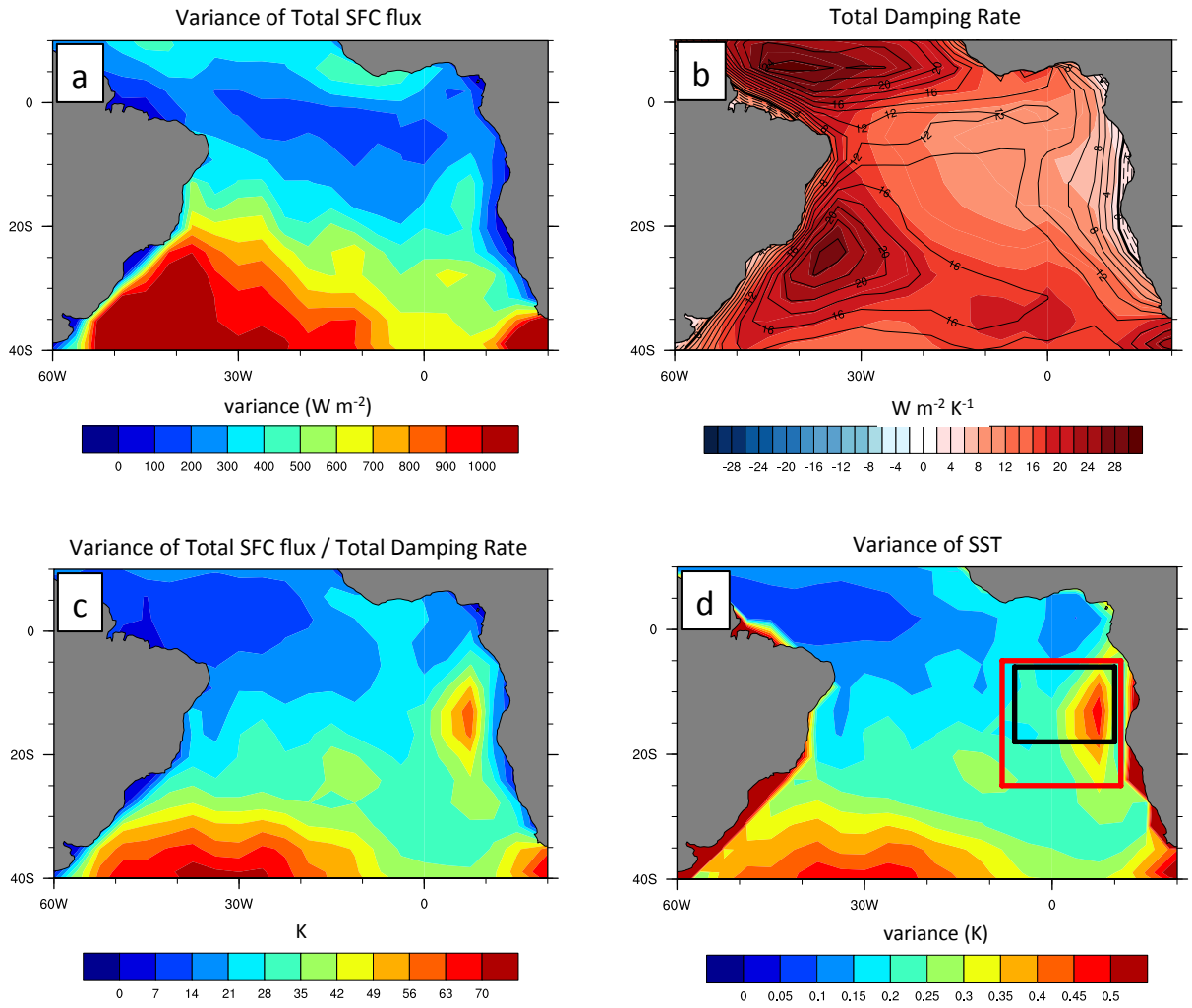

Figure 15. (a) Variance of the sum of the net surface fluxes (long-wave + short-wave + latent + sensible); (b) Damping rate of net surface fluxes computed as in Park et al. (2005). Contours indicate the damping rate of LHF only; (c) Variance of net surface fluxes divided by their damping rate; (d) Variance of SST in the control simulation (same as in fig. 5a). Superimposed are (red) box of the Namib experiment and the (black) box of the Box 6 experiment.